LBL-24497 c.2

# Lawrence Berkeley Laboratory
UNIVERSITY OF CALIFORNIA

## Physics Division

RECEIVED
LAWRENCE
BERKELEY LABORATORY

APR 12 1988

LIBRARY AND
DOCUMENTS SECTION

To be published in the Proceedings of the Workshop on Experiments, Detectors, and Experimental Areas for the SSC, Berkeley, CA, July 7–17, 1987

# Detecting the Heavy Higgs Boson at the SSC

R.N. Cahn, M. Chanowitz, M. Golden,
M.J. Herrero, I. Hinchliffe, E.M. Wang,
F.E. Paige, J.F. Gunion,
and M.G.D. Gilchriese

December 1987

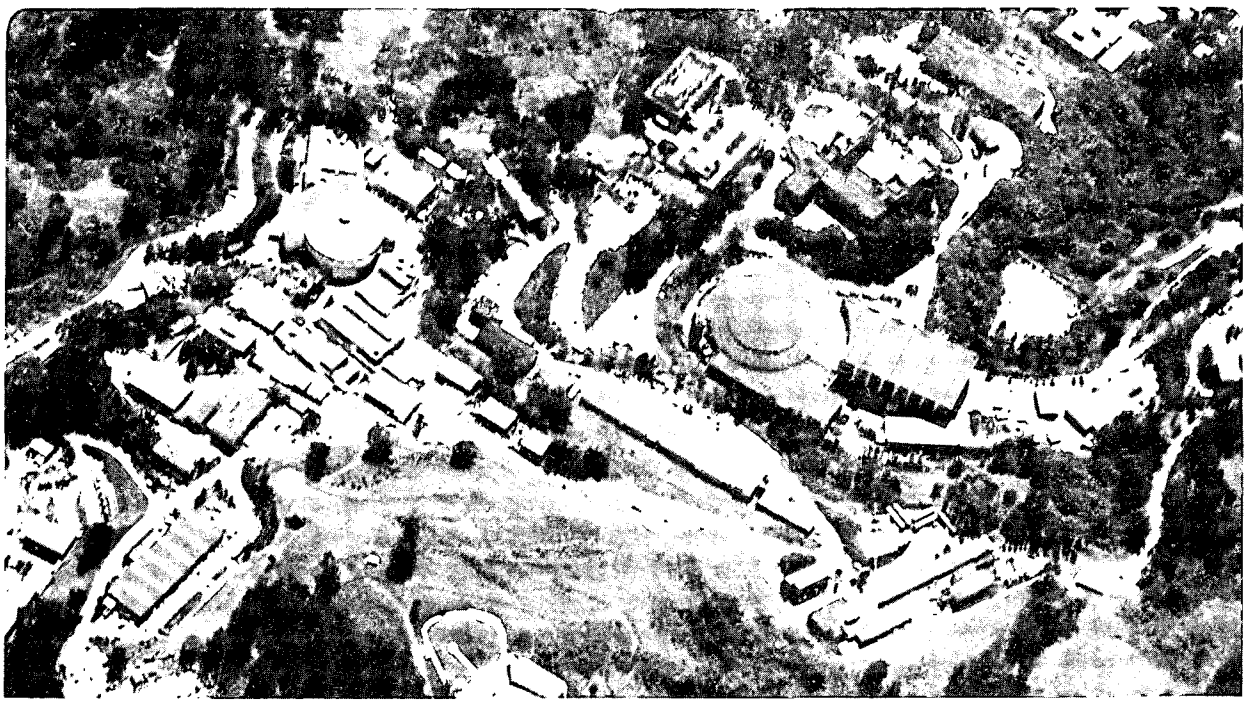

Prepared for the U.S. Department of Energy under Contract DE-AC03-76SF00098

LBL-24497 c.2

## DISCLAIMER

This document was prepared as an account of work sponsored by the United States Government. While this document is believed to contain correct information, neither the United States Government nor any agency thereof, nor the Regents of the University of California, nor any of their employees, makes any warranty, express or implied, or assumes any legal responsibility for the accuracy, completeness, or usefulness of any information, apparatus, product, or process disclosed, or represents that its use would not infringe privately owned rights. Reference herein to any specific commercial product, process, or service by its trade name, trademark, manufacturer, or otherwise, does not necessarily constitute or imply its endorsement, recommendation, or favoring by the United States Government or any agency thereof, or the Regents of the University of California. The views and opinions of authors expressed herein do not necessarily state or reflect those of the United States Government or any agency thereof or the Regents of the University of California.

# Detecting the Heavy Higgs Boson at the SSC*

R.N. Cahn, M. Chanowitz, M. Golden, M.J. Herrero
I. Hinchliffe and E.M. Wang
Lawrence Berkeley Laboratory
University of California
Berkeley, CA 94720

F.E. Paige
Brookhaven National Laboratory
Upton, NY 11973

J.F. Gunion
Department of Physics
University of California
Davis, CA 95616

M.G.D. Gilchriese
SSC Central Design Group
Lawrence Berkeley Laboratory
University of California
Berkeley, CA 94720

## Abstract

Detection of a heavy Higgs boson ($2M_z < M_H < 1$ TeV) is considered. The production mechanisms and backgrounds are discussed. Their implementation in the PYTHIA and ISAJET Monte Carlo programs are checked. The decay modes $H \to ZZ \to llll$ and $H \to ZZ \to ll\nu\nu$ are discussed in detail. The signal/background is evaluated and some relevant detector parameters are specified. Some remarks are also made concerning the requirements imposed on detectors by the decay mode $H \to WW \to l\nu + jets$. Experimental signatures for models in which there is no Higgs boson of mass less than 1 TeV are outlined.

* This work was supported in part by the Director, Office of Energy Research, Office of High Energy and Nuclear Physics, Division of High Energy Physics of the U.S. Department of Energy under Contracts DE-AC03-76SF00098 and DE-AC02-76CH00016.

## 1. Theoretical Introduction

A central motivation for the SSC is to study the mechanism of electroweak symmetry breaking which gives the $W$ and $Z$ their masses. Though the general framework is believed to be the Higgs mechanism, essentially nothing is known about the details. There may be a single Higgs boson as in the minimal standard model;[1] there may be several Higgs bosons as in supersymmetric theories;[2] or there may be pseudoscalar bound states as in some technicolor models.[3] The mass scale is equally uncertain and could be anywhere from a few GeV to the TeV range. Two points are assured by the general framework. First, there are new particles carrying a new force which induces the spontaneous breaking of the electroweak $SU(2)_L \times U(1)$ gauge invariance. Second, the new force causes strong scattering of longitudinally polarized $W$'s and $Z$'s if the mass scale of the associated new particles is of order 1 TeV or higher.

If the mass scale of symmetry breaking physics is above the $WW$ and $ZZ$ thresholds, then it can be studied at the SSC in events containing $W^+W^-$, $ZZ$, and in some cases $W^\pm Z$, $W^+W^+$, or $W^-W^-$ pairs. In the standard model with a Higgs boson mass $m_H \lesssim 600$ GeV, the Higgs boson appears as a resonance in the $W^+W^-$ or $ZZ$ channels with a width of less than 100 GeV. Since the width grows like $m_H^3$, for larger values of $m_H$, the Higgs signal is an excess of $W^+W^-$ and $ZZ$ pairs over the $WW$ or $ZZ$ continuum. There is no easily recognizable peak in the mass spectrum. More generally, arguments based on unitarity show that symmetry breaking physics will be manifested in 1-2 TeV gauge boson pairs if it does not occur at a lower mass scale.[4] Detection of gauge boson pairs is therefore a critical requirement for SSC physics.

In this paper we briefly discuss the significance of the 1 TeV mass scale (Section 2), production mechanisms and decay properties of the standard heavy Higgs (Section 3), comparison of existing Monte Carlo programs with theory (Section 4), and results on the experimental detection of the heavy Higgs signal in a variety of modes (Sections 5, 6 and 7). In Section 8 we attempt to summarize the relevant desirable detector properties that are indicated by our study.

It should be noted that the studies of experimental requirements are not complete in the sense that definitive studies of signal-to-background ratios have not yet been made for all decay modes of the heavy Higgs. Nevertheless, we believe that it is possible to indicate with some confidence the necessary detector parameters required to observe the relevant signals and to reject backgrounds.

## 2. Significance of the TeV Scale

The 1–2 TeV scale plays a special role in the physics of electroweak symmetry breaking. First it defines the onset of strong interactions: if the typical mass scale

$M_{SB}$ of the quanta of the symmetry breaking sector is 1 TeV or heavier, then the symmetry breaking interaction is strong. Second, as explained more precisely below, 1–2 TeV is the maximal energy scale at which the effects of the symmetry breaking must begin to emerge. In this sense it is like the 300 GeV limit of the Fermi theory of weak interactions. Unitarity requires that, at this energy scale or below, the Fermi theory would be supplanted by new physics as indeed occurred with the discovery of the $W$ and $Z$.

The first of these points is easily illustrated in the minimal standard model with a single Higgs boson.[1] The lowest order relationship between the coupling constant $\lambda$, the Higgs boson mass $m_H$, and the vacuum expectation value $v$, is

$$\lambda = \frac{m_H^2}{2v^2}. \tag{1}$$

Quantum corrections are typically of order $\lambda/4\pi$ and are $O(1)$ for strong coupling, *i.e.*, if $m_H \cong \sqrt{8\pi}v \cong 1$ TeV. More precisely, unitarity fails in leading order for $m_H \cong 1$ TeV, indicating the onset of strong interactions since large quantum corrections must then arise to restore unitarity.[5]

A model-independent approach is based on symmetry principles first used in hadron physics. Just as the pion is a Goldstone boson associated with the spontaneous breaking of chiral symmetries in QCD, so the longitudinal modes $W_L$ and $Z_L$ are essentially (at energies large compared to $M_W$) Goldstone bosons arising from the breaking of gauge symmetries. The same techniques that establish pion low energy theorems,[6] such as

$$a_0(\pi^+\pi^- \to \pi^0\pi^0) = \frac{s}{16\pi F_\pi^2} \tag{2}$$

for the $J = 0$ partial wave amplitude can also be used to show that [4]

$$a_0(W_L^+W_L^- \to Z_LZ_L) = \frac{\hat{s}}{16\pi v^2} \tag{3}$$

Eq. (2) is valid for $s \ll m_{\text{hadron}}^2$ while Eq. (3) applies for $M_W^2 \ll \hat{s} \ll M_{SB}^2$ and can therefore only be relevant if $M_{SB} \gg M_W$. In that case it shows that new physics must intervene below $\sqrt{16\pi v^2} = 1.8$ TeV to preserve unitarity, $a_0 \leq 1$. Eq. (3) also shows that if $M_{SB} \geq 1$ TeV, then for $\sqrt{\hat{s}} \approx 1$ TeV, $a_0$ will be O(1) which is the precise indication of strong scattering (for instance, putting $\hat{s} \geq 1$ TeV$^2$ in Eq. (3) we find $a_0 \geq 1/3$).

The search for the mechanism of symmetry breaking is therefore not open-ended. Unlike new gauge bosons, $W'$ or $Z'$, which might exist at arbitrarily heavy

masses or might not exist at all, the symmetry breaking sector must exist and will manifest its presence at least indirectly in strong $W_L$, $Z_L$ scattering at $\hat{s} \gtrsim 1$ TeV$^2$ unless the mass scale $M_{SB}$ is below 1 TeV.

## 3. Calculation of Higgs Production Cross Sections

Higgs production may result from gluon-gluon fusion via a heavy quark loop[7] (Fig. 3.1a) by quark-antiquark annihilation (Fig. 3.1b) and by gauge boson fusion[8] (Fig 3.1c). The first two of these depend strongly on the $t$ quark mass — see Fig. 3.2 taken from Ref. 9 for an indication of this dependence. Note that a larger $t$ mass generally implies a larger Higgs production cross section. For Higgs masses below about 600 GeV and above 2 $M_Z$, discovery of the Higgs is straightforward in the channel $H \to ZZ$, both Z decaying to $e^+e^-$ or $\mu^+\mu^-$ as we will show in Section 5. One is therefore less sensitive to uncertainties in the theoretical calculations of the cross section, mostly due to the unknown $t$-quark mass which affects the gluon-gluon fusion process. Since most of our calculations have been done for a $t$ quark mass of 40 GeV, we are somewhat conservative

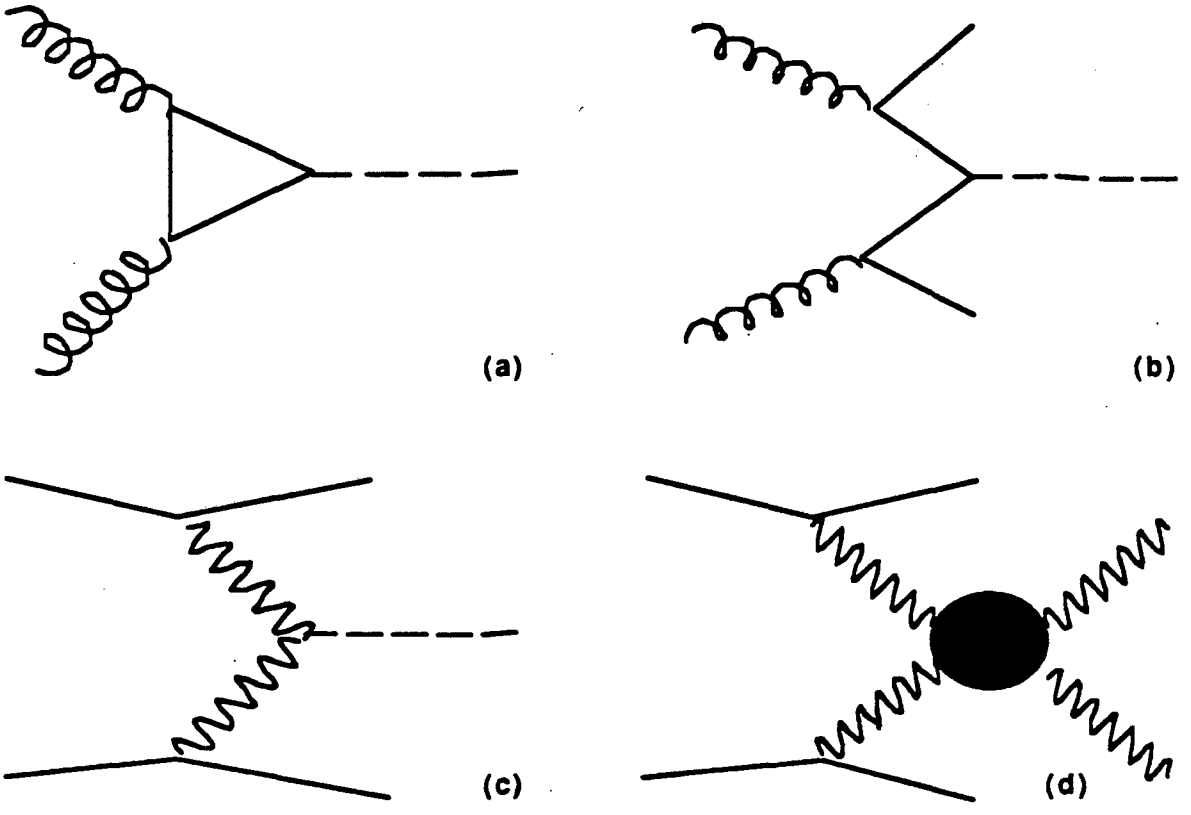


3.1 Higgs production via (a) gluon-gluon fusion; (b) quark-antiquark annihilation; (c) $WW$ or $ZZ$ fusion; and (d) production of gauge boson pairs in a theory with a strongly coupled gauge boson sector.

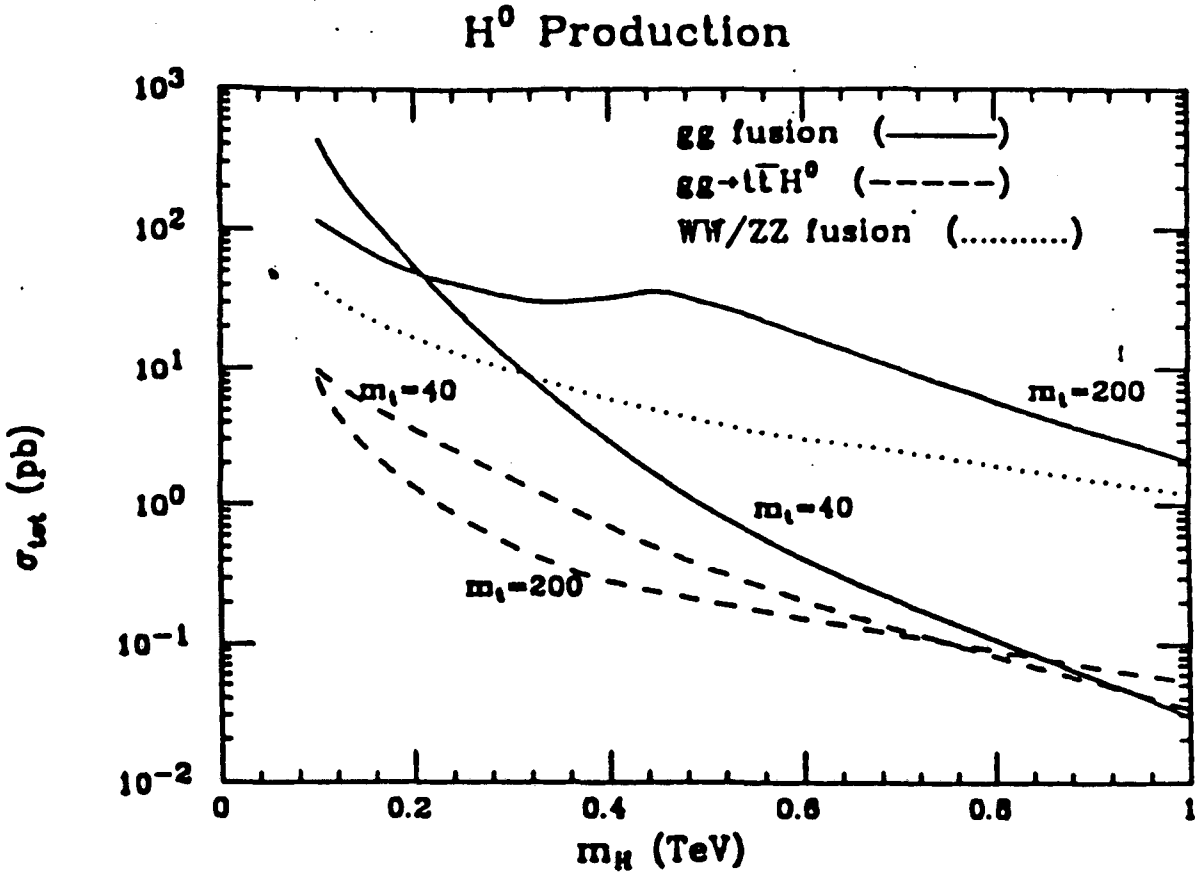


3.2 The Higgs production cross sections from the various processes discussed in the text as a function of the Higgs mass for two different $t$ quark masses (taken from Ref. 9).

given present limits on the $t$ quark mass. The situation for Higgs heavier than about 600 GeV is less clear and therefore we discuss in more detail below the theoretical calculations relevant to this region.

In the published literature a variety of different approximations have been used to compute Higgs production by $WW$ and $ZZ$ fusion. The effective $W$ approximation[4,10] is analogous to the effective photon or Weizsacker-Williams approximation used for photon-photon scattering. It is a small scattering angle approximation which neglects the $P_T$ of the scattered quarks and therefore also of the produced Higgs boson, both characteristically of order $M_W$. It provides a sufficiently accurate approximation to the total cross section for Higgs mass from 500 GeV and up, with errors of about 10%.[11]

A second common approximation is to include only the $s$-channel Higgs pole diagram calculated in a particular gauge ($U$-gauge);[8,28]

$WW$ or $ZZ \to H \to WW$ or $ZZ$

This approximation neglects $t$ and $u$ channel Higgs exchanges, if present, and also neglects gauge sector exchange diagrams. This approximation is pathological since in $U$-gauge good high energy behavior is obtained by cancellation of badly behaved contributions from the Higgs and gauge sectors. This is not a serious problem for Higgs masses $m_H \lesssim 600$ GeV for which the width is reasonably narrow, since the signal in the peak is not seriously affected by the bad high energy behavior. For the 1 TeV Higgs boson with $\Gamma_H \sim \frac{1}{2}$ TeV there is no recognizable peak and it is necessary to integrate over a broad range of $WW$ and $ZZ$ invariant masses. The $s$-channel $U$-gauge pole approximation then seriously overestimates the high mass tail and the production cross section, as discussed in detail in Section 4 below.

Two approaches can be used to overcome this problem. One is to do a complete calculation, including the gauge sector contributions.[29] The other is to calculate the Higgs sector contributions in a renormalizable gauge (justified by the equivalence theorem[4,13]) which automatically has the correct high energy behavior. This is computationally simple since the difficult gauge sector contributions are not included. In the central region (away from the singularity of the Coulomb exchange pole) they may be safely neglected.[14] Numerically the approximation is very good [15] for $m_H = 1$ TeV and $m_{WW} \geq 0.8$ TeV, which is the region in which the signal emerges from the $\bar{q}q$ background. Because of its simplicity, the $R$-gauge approach can be a useful check of the "exact" $U$-gauge computations.

Higgs production is sometimes also computed in the zero-width approximation, as if the Higgs were a stable particle.[8,11,23] This is probably reliable for the range of Higgs masses below $\sim 600$ GeV corresponding to "narrow" peaks but fails around $m_H = 1$ TeV. In the latter case, the signal can only be seen over the $\bar{q}q$ background on the high side of the "peak" where it suffers from falling luminosity that is not reflected in the zero-width computation.

Finally, we should remember that for $m_H = 1$ TeV the Higgs sector is strongly interacting and therefore cannot really be described by perturbation theory. Therefore even the "exact" $U$-gauge calculation should be regarded as heuristic in this case. There is however evidence that perturbation theory is not a completely misleading guide to Higgs production at $m_H = 1$ TeV: the Higgs sector one loop contributions only correct $\Gamma_H$ by 10% at $m_H = 1$ TeV.[16]

### 3.1 Strongly Interacting $W$ and $Z$ Bosons

The $WW$ fusion process of Fig. 3.1d is the source of the signal for strong $W_L$, $Z_L$ scattering. This is a generalization of one of the Higgs production mech-

anisms discussed above. The strong interactions, represented by the blob in Fig. 3.1d, generate an excess of gauge boson pairs over those produced by $q\overline{q}$ and $gg$ annihilation. The presence of gauge boson pairs with invariant mass greater than about 1 TeV is the signal for a strongly coupled symmetry breaking sector. The yield of these pairs can be estimated by modeling the gauge boson scattering amplitude as discussed in Section 2 and Ref. 4.

In addition to the neutral pairs, $W^+W^-$ and $ZZ$, which are also produced by decay of a ($M_H < 1$ TeV) Higgs boson, a strongly coupled theory will produce charge 1 ($ZW$) and 2 ($W^\pm W^\pm$) final states.[4,17] The latter is particularly important since it has a much smaller background; $W^\pm W^\pm$ cannot be produced by $q\overline{q}$ annihilation. Many of the background issues relevant to Higgs detection are applicable to this case. Some backgrounds (e.g., the background from $Z+$jets to the $ZZ \to ee\nu\nu$ mode) may be relatively less important since the invariant mass of the boson pair is larger. Since models for a strongly coupled weak sector are not included in the ISAJET[18] and PYTHIA[19] Monte Carlo programs, we have not yet performed a detailed analysis of these signals.

### 3.2 $\overline{q}q$ Annihilation Background

The processes [20,21] $\overline{q}q \to WW$, $ZZ$ are a serious background to $H \to WW$, $ZZ$ detection in all $WW$, $ZZ$ decay channels.† The gauge bosons produced by $\overline{q}q$ annihilation are predominantly transversely polarized while those from the Higgs decay are predominantly longitudinal.

For Higgs boson masses less than 0.6 TeV, for which there is a recognizable invariant mass peak, it is less critical to know the backgrounds precisely. At the SSC the Higgs boson in this mass range emerges as a peak in the $ZZ \to e^+e^-/\mu^+\mu^- + e^+e^-/\mu^+\mu^-$ channel over the smooth $\overline{q}q$ background. However for the 1 TeV Higgs boson and for the 1-2 TeV strong interaction signal discussed above, there is no peak and it is important to understand the magnitude of the $\overline{q}q$ background.

There are two ingredients in a calculation‡ of the background; perturbative QCD calculations of the relevant partonic process; and a set of structure functions. The first is the easier to deal with. There is $Q^2$-dependence in both $\alpha_s(Q^2)$ and $f(x, Q^2)$. For the production of $W$ or $Z$ pairs of invariant mass $M$, $Q \approx M$. The relevant processes are $q + \overline{q} \to Z + Z$[21] and $g + g \to Z + Z$.[22] Until recently only the former was calculated. The QCD corrections to this process which occur

† Recently, the process $gg \to ZZ$ has been computed.[22] Although this process was not included in our simulations, we shall comment on its effect when it is appropriate.

‡ Previous studies of this process were carried out by Eichten, Hinchliffe, Lane and Quigg,[23] by Owens,[24] by Tung[25], by Collins[26] and by Collins and Soper.[27]

at order $\alpha_s$ are not known, but the calculation is not difficult. It is very likely that they will be known by the time SSC data are available. In the absence of this calculation, there is an uncertainty of order 30% in the background from this source. The second process, gluon-gluon production, which is of order $\alpha_s^2$ is also important. This process is approximately 50% of $q\overline{q}$ annihilation provided $|y_z| < 1.5$. Again it is expected that the order $\alpha_s^3$ corrections will be small, although the calculation is formidable.

The uncertainties in structure functions present a more serious problem. Structure functions are measured in low $Q^2$ experiments and then extrapolated in $Q^2$ up to the appropriate scale. There are three main problems:

1) the appropriate value of $\Lambda$ must be determined.
2) There is little data for $x < 0.1$ and no data at all for $x < 0.01$.
3) The gluon distribution which produces most of the antiquarks at high $Q^2$ is not measured directly but is inferred from the growth of the antiquarks with $Q^2$ and is therefore correlated with $\Lambda$.

In the case of the $W$ or $Z$ pair background, one is interested in $M$ between 200 GeV and 2 TeV. For central production this corresponds to values of $x$ between 0.005 and 0.05. To a first approximation† the structure functions depend only on $Q^2/\Lambda^2$. Consequently the uncertainty due to errors in $\Lambda$ can be estimated by shifting $Q^2$. A look at the $Q^2$ dependence of the structure functions will show that the $Q^2$ dependence is small over the range of $x$ that we are interested in (see EHLQ[23] Figs. 10–15). A sample is reproduced here as Fig. 3.3. Effect (3) was discussed in EHLQ where two different sets of gluon distributions at $Q^2 = 5$ GeV$^2$ were used (compare EHLQ Figs. 5 and 6). These different sets produced changes of less than 20% for all the SSC rates in EHLQ.

Problem (2) was also addressed by EHLQ who modified the structure functions below $x = 0.01$ (see EHLQ Eqs. 2.62 and 2.63 and Figs. 18–20). The effects wash out rapidly at $Q^2$ rises, and are, of course irrelevant for $x > 0.01$.

To verify experimentally these background calculations, a process that is sensitive to the same quark distributions as the background over the same range of $x$ and $Q^2$ is needed. The only process available are dilepton production and the production of two large $P_T$ photons. $W$ or $Z$ production is less useful since the total cross section is dominated by values of $x$ that are much smaller than the relevant ones and $Q^2$ is also smaller. By looking at $W$'s at large rapidity one becomes sensitive to the product of two distribution functions; one in the interesting $x$ range and one at much smaller $x$. Jet cross sections are not useful since for total transverse energies below 6 TeV, gluon-quark and gluon-gluon scattering dominate.

† This is not quite true since there are quark mass effects, but these changes are very small unless one is sensitive to heavy (top) quark distributions.

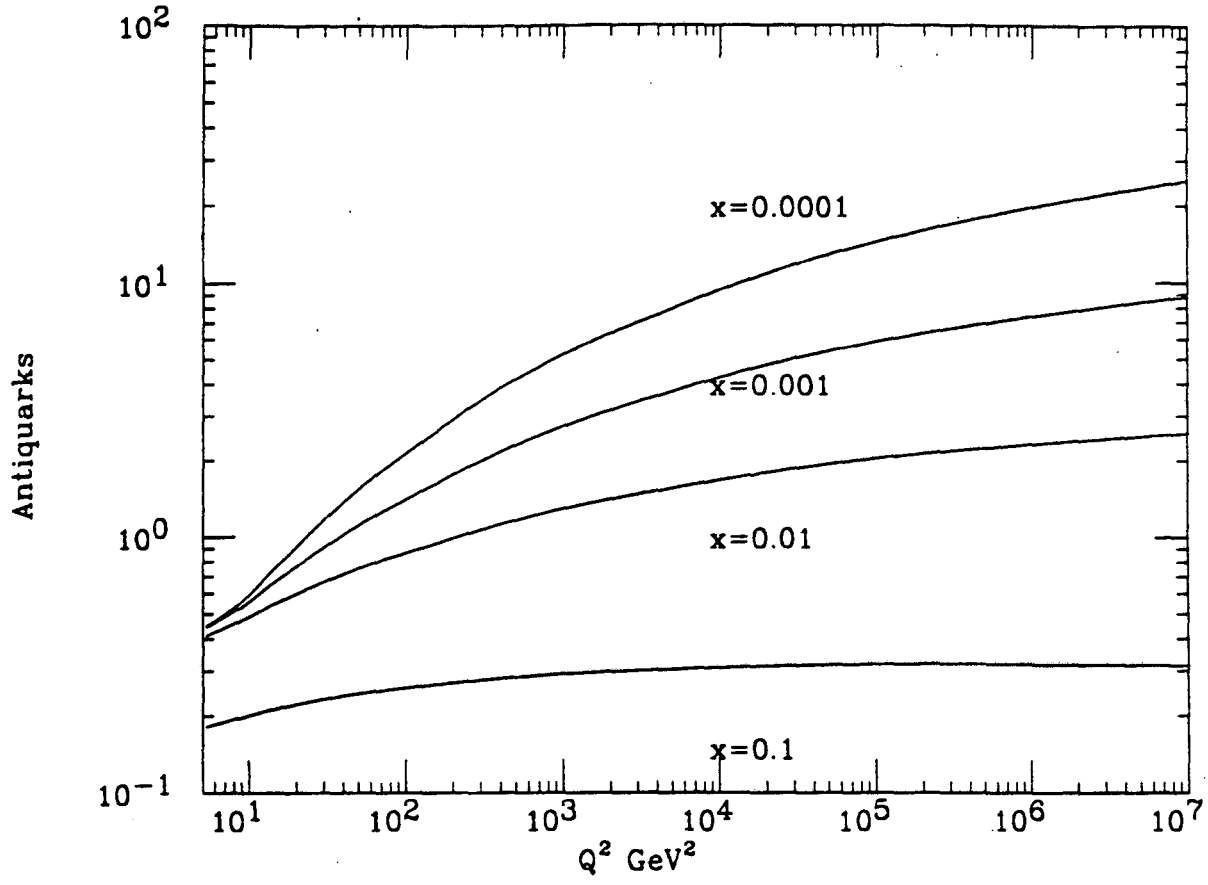


**3.3 The $Q^2$ dependence of the antiquark distribution at fixed $x$.**

How well can dilepton production be measured? Figure 3.4 shows the event rate which must be measured over the same range of invariant mass that will be needed for $W$ pairs. At dilepton pair masses of 1 TeV there are enough events in a 50 GeV bin to make a 30% measurement in each bin. There will also be an error on the measurement of the dilepton mass. A 5% error on this measurement translates into a 15% error on the cross-section. This figure attempts to indicate the effect of uncertainties in structure functions; changes in $\Lambda$ from 150 to 450 MeV are too small to measure.

A new set of structure functions has been invented that attempts to increase the dilepton rate (and also the $W$ or $Z$ pair background). The EHLQ structure functions at $Q^2 = 5$ GeV$^2$ have been changed as follows. Take set 2 of EHLQ and double the sea i.e., assume that the measurements of the antiquarks are a factor of 2 too small at low $Q^2$. Replace the gluon distribution (EHLQ 2.60) by

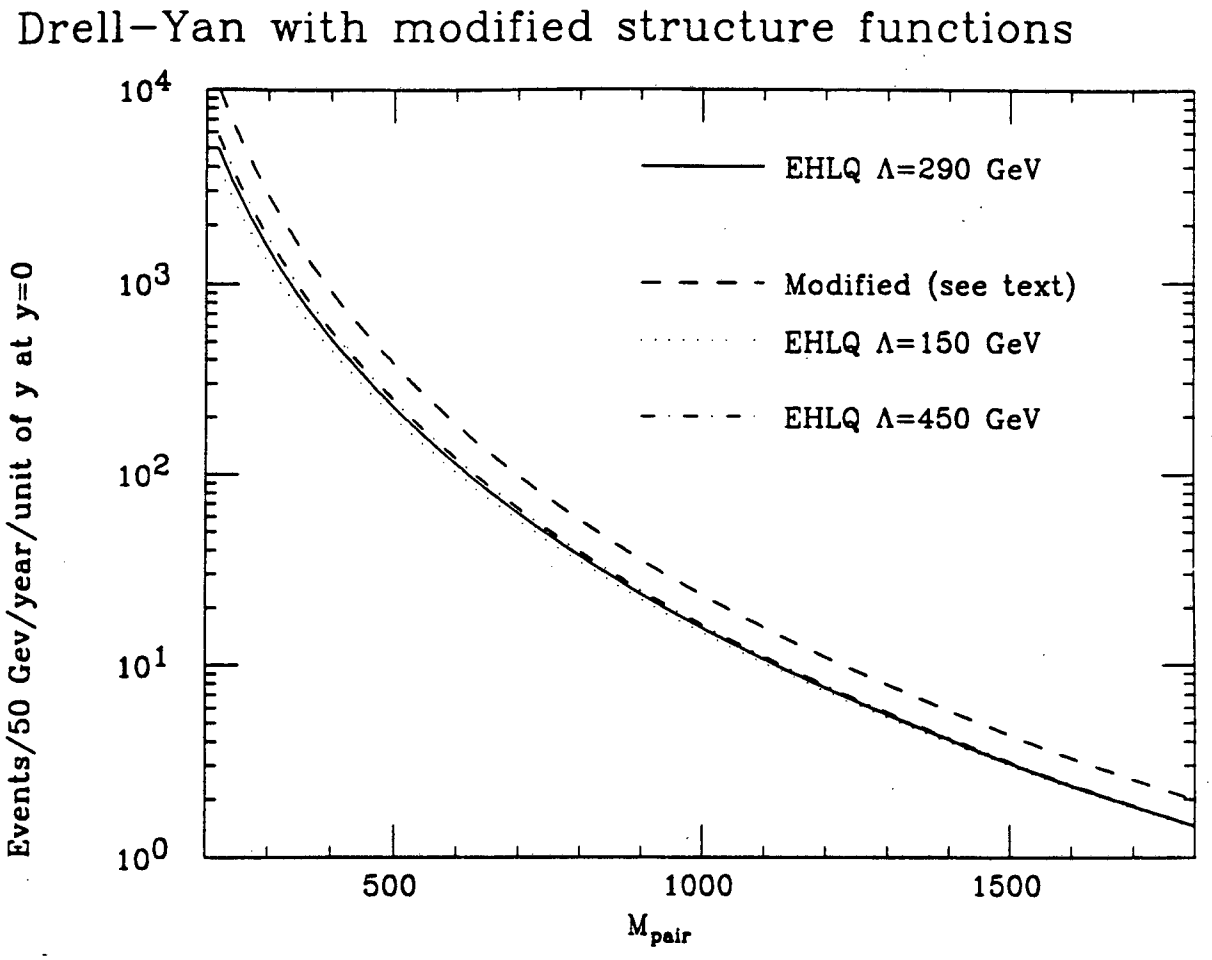


**3.4** The cross section $d\sigma/dmdy$ for the production of a muon pair at $y = 0$ as a function of the muon pair invariant mass. Four curves are shown; three of these use the EHLQ set 2 structure functions with different choices for $\Lambda_{QCD}$. The fourth curve corresponds to the modified set of structure functions described in Section 3.2.

$$xg(x, 5\text{GeV}^2) = 2.6(1-x)^4 \quad ; \quad x > 0.1$$

$$xg(x, 5\text{GeV}^2) = 0.54/\sqrt{x} \quad ; \quad x < 0.1$$

This set of structure functions has a much more singular behaviour at small $x$ than EHLQ's and is similar at larger $x$. These changes are unlikely to be in agreement with current data. In particular, they are likely to generate too large a value for $F_2(x, Q^2)$ at $Q^2 \sim 20$ GeV$^2$ for $x \sim 0.05$ where data exist. They also violate the constraint that the total momentum carried by partons must add up to one. This modified set is compared with EHLQ set 2 structure functions in Fig. 3.5. Figure 3.4 shows the effect of these structure functions on the dilepton

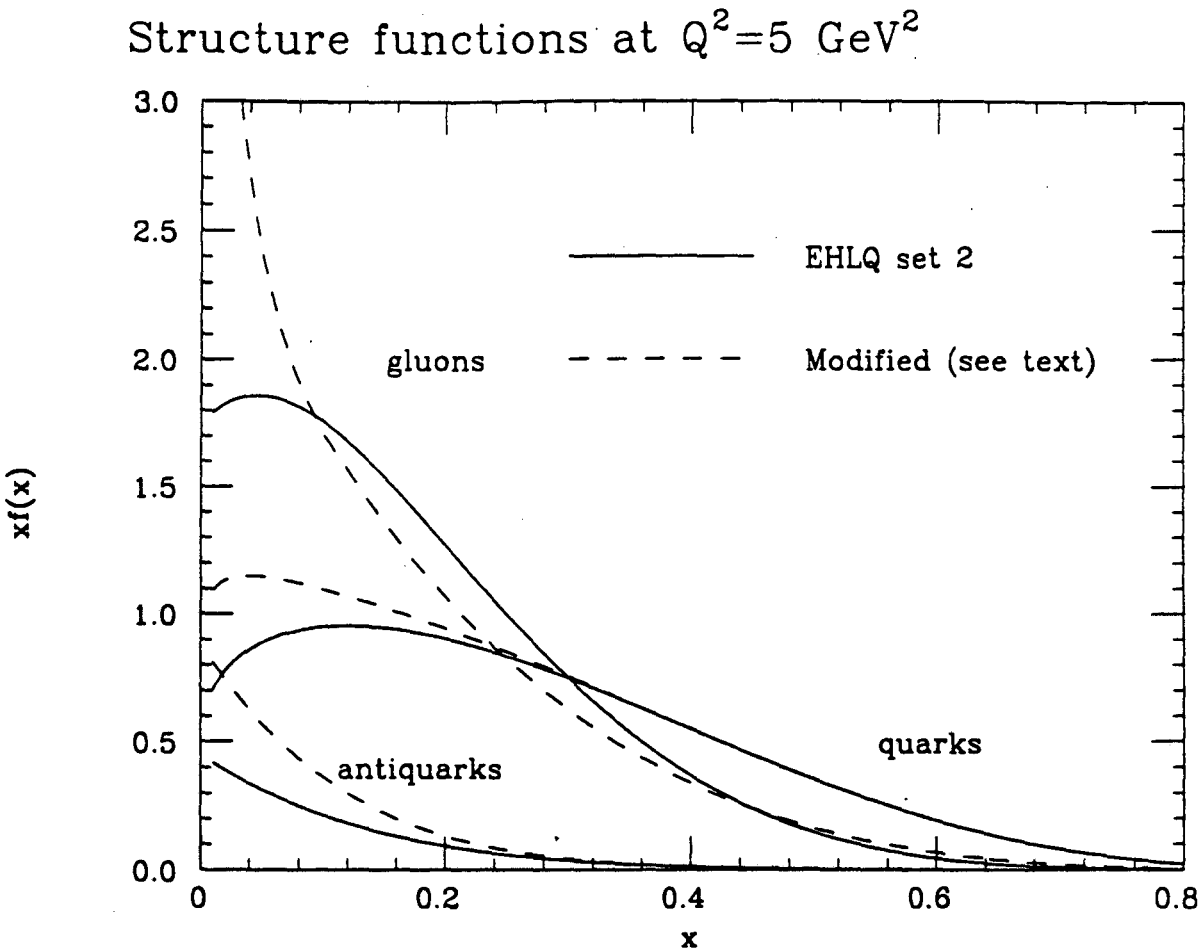


**3.5 The quark, antiquark and gluon distributions as a function of $x$ at $Q^2 = 5$ GeV$^2$. Two sets are shown; those of EHLQ set 2 and those described in Section 3.2.**

rate. The effect is greatest at small values of the dilepton mass where $x$ and $Q^2$ are smallest. It is likely that this process can be measured well enough to see the difference between this result and the EHLQ prediction.

Figure 3.6 shows the $Z$ pair rate using the same structure functions as Fig. 3.5. The relative contributions of the charge 1/3 and charge 2/3 quarks to the dilepton and $Z$ pair processes are not quite the same. Hence it is conceivable that one could be affected more than the other by changes in structure functions. Nevertheless is very difficult to double the $Z$ pair rate while keeping the dilepton rate unchanged. In practice, a large number of processes will be measured, all of which contribute to the knowledge of structure functions. This will surely allow some of the remaining uncertainties to be eliminated. There will be enough dilepton events to provide a calibration of the background at the 60% level over

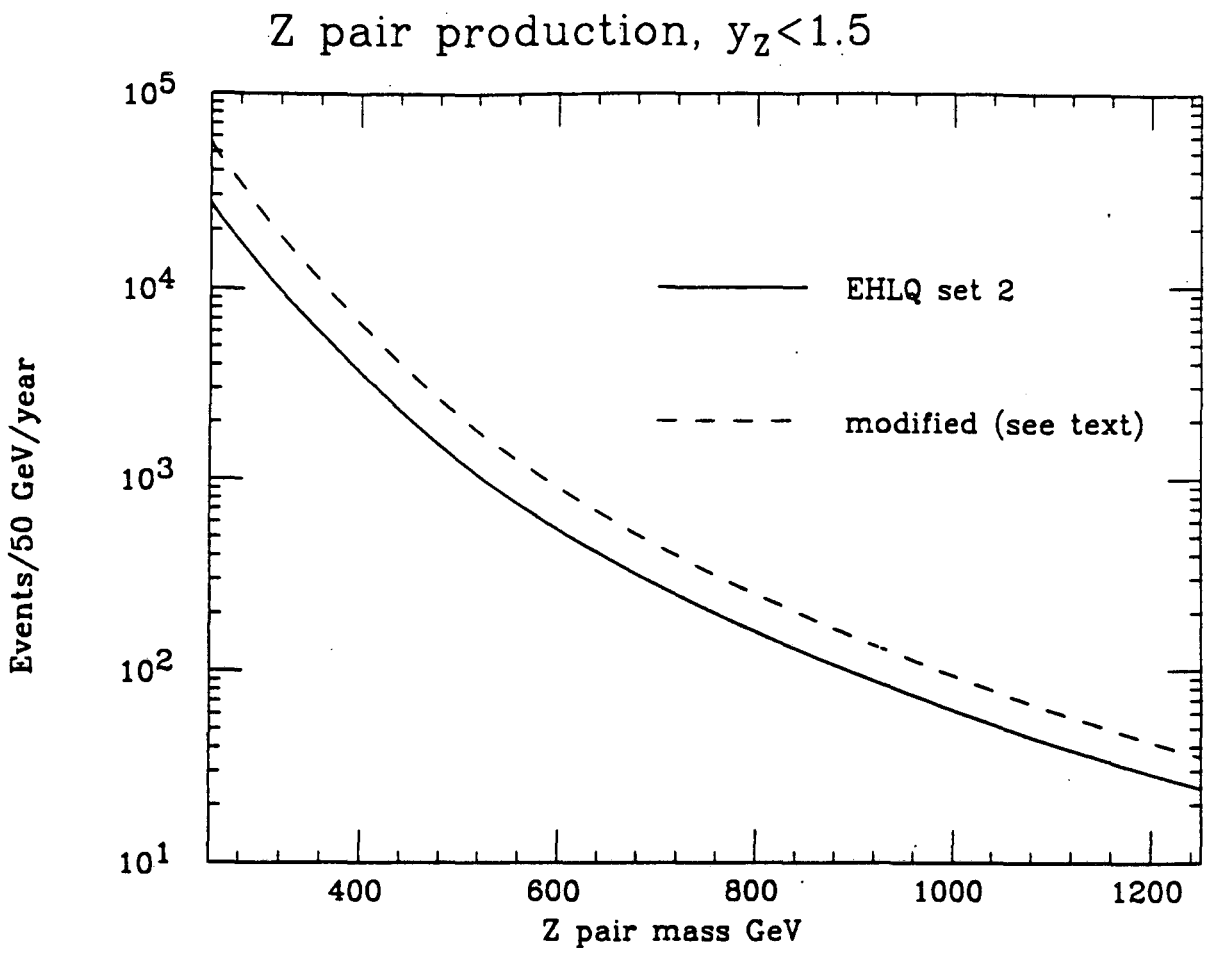


**3.6** The cross section $d\sigma/dM$ for the production of a $Z$ pair of mass $M$. Both $Z$'s are required to have $|y_Z| < 1.5$. The two lines show the effect of different sets of structure functions; EHLQ set 2 and those described in Section 3.2.

the range of $Z$ pair masses less than 1 TeV or so. At larger $Z$ pair masses the situation is more difficult. There are only about 25 dilepton pairs with invariant mass greater than 1.5 TeV, so it becomes difficult to measure the background over the relevant range of $x$ and $Q^2$. Nevertheless, it is very unlikely to be uncertain to more than a factor of two.

## 4. Higgs Production Processes: Comparison Between Theory and Monte Carlo Programs

In this section we test the predictions of the ISAJET[18] (v5.34) and PYTHIA[19] (v4.8) Monte Carlo programs against simple partonic calculations.

### 4.1 Signal

The Higgs production processes that are included in ISAJET and PYTHIA are (1) quark-antiquark annihilation; (2) gluon-gluon fusion via a heavy quark loop; and (3) gauge boson fusion. The strength of processes 1 and 2 are highly dependent on the top quark mass — see Section 3.

Process 1 is never a significant source of Higgs bosons compared to processes 2 and 3. It is, however, treated poorly by ISAJET and PYTHIA. The problem is the following: since the coupling of a quark to the Higgs boson is proportional to the quark mass, the only quark flavor that contributes appreciably is top. There will be, therefore, a top-antitop pair in the proton fragments going down the beam pipe. When the top quark is heavy, this contributes a suppression not included in the naive computation using the EHLQ structure functions. Therefore, process 1 may be overestimated when the top quark is not substantially lighter than the Higgs. A more correct computation valid for any reasonable top quark mass is to include this process in the form of Fig. 3.1b. However, for the range of Higgs masses considered (400 GeV $< M_H <$ 800 GeV) and the top quark mass of 40 GeV, the approximations used by ISAJET and PYTHIA are acceptable.

Gluon-gluon fusion is appreciable for a light Higgs. If the top quark weighs 40 GeV, it is the dominant process for $M_H$ below about 350 GeV. If the top quark is as heavy as 150 GeV, gluon-gluon fusion will dominate up to a Higgs mass of about 900 GeV. Above these values, the Higgs boson is produced largely by the gauge boson fusion mechanism.[8,10]

In order to check that ISAJET and PYTHIA treat gluon-gluon fusion properly, their rates for this process were compared with the results of a program that computes the partonic cross section. This program was written by the authors of Ref. 23. Table 4.1 shows the results. Here and below, one SSC year corresponds to an integrated luminosity of $10^{40}\text{cm}^2$. The $gg$ fusion cross section in ISAJET v5.34 was wrong, but has since been corrected. The corrected results are given in Table 4.1.

In considering the Higgs production via gauge boson fusion it is important to note that the Higgs itself is not a final state particle, but rather a resonance that immediately decays into $W$ or $Z$ pairs. Therefore what one must actually calculate is the process $qq \to qqVV$, where $V$ is $W$ or $Z$. The complete gauge invariant calculation of this process[29] is quite difficult and the resulting matrix element is too unwieldy to be used in a Monte Carlo program.

**Table 4.1**

A comparison of the event rates for the process $gg \to H \to ZZ$ from the corrected version of ISAJET, PYTHIA and a partonic calculation *ala* EHLQ. No rapidity cuts are applied. Events per SSC year are shown.

| $M_H$ | ISAJET | PYTHIA | Partonic |
|---|---|---|---|
| 400 | 6200 | 7800 | 7600 |
| 800 | 210 | 260 | 260 |

ISAJET and PYTHIA treat the $qq \to qqVV$ process using the effective-$W$ approximation as described in Section 3. In this approximation, the incoming gauge bosons are treated as though they were constituents of the incoming protons. One can then compute a luminosity distribution for $V$ pairs. This is then multiplied by the on-shell matrix element for $VV \to VV$.

ISAJET and PYTHIA take two different approaches to the computation of this matrix element. ISAJET computes the full set of $VV \to VV$ diagrams. Only longitudinally polarized incoming $V$'s are included, though all polarizations are included on the outgoing legs. PYTHIA computes only the $s$-channel Higgs pole diagram and only longitudinal polarizations are included in the final state. (PYTHIA is being revised to perform the same computation as ISAJET).[30]

Each of these approximations has its pathologies. The effective-$W$ approximation treats the incoming $V$'s as being on mass shell while in fact they are off mass shell by approximately their mass. The net effect of this is to overestimate the total rate somewhat, especially for a Higgs near the $H \to VV$ threshold.

The approximation made by ISAJET suffers in the $W^+W^-$ channel from having a fictitious $t$-channel photon exchange pole caused by putting the incoming bosons on mass shell. This leads to an infinite total cross section. One must therefore always impose some minimum $P_T$ cut on the outgoing particles. If $P_T$ is at least of order the $W$ mass, then the ISAJET's result should approximate the true answer. In any case, such a cut is required to reduce the background.

PYTHIA's approximation does not have a fictitious infinity at low $P_T$, because the photon exchange diagram is not included. However, the $s$-channel Higgs exchange diagram by itself is not gauge invariant, and it violates unitarity at high energy. Examples of this are shown in Figs. 4.1a-c. These figures show the cross section for unpolarized $ZZ \to ZZ$ scattering at Higgs masses of 400, 800, and 1000 GeV. For $ZZ \to ZZ$ scattering there are three diagrams. The

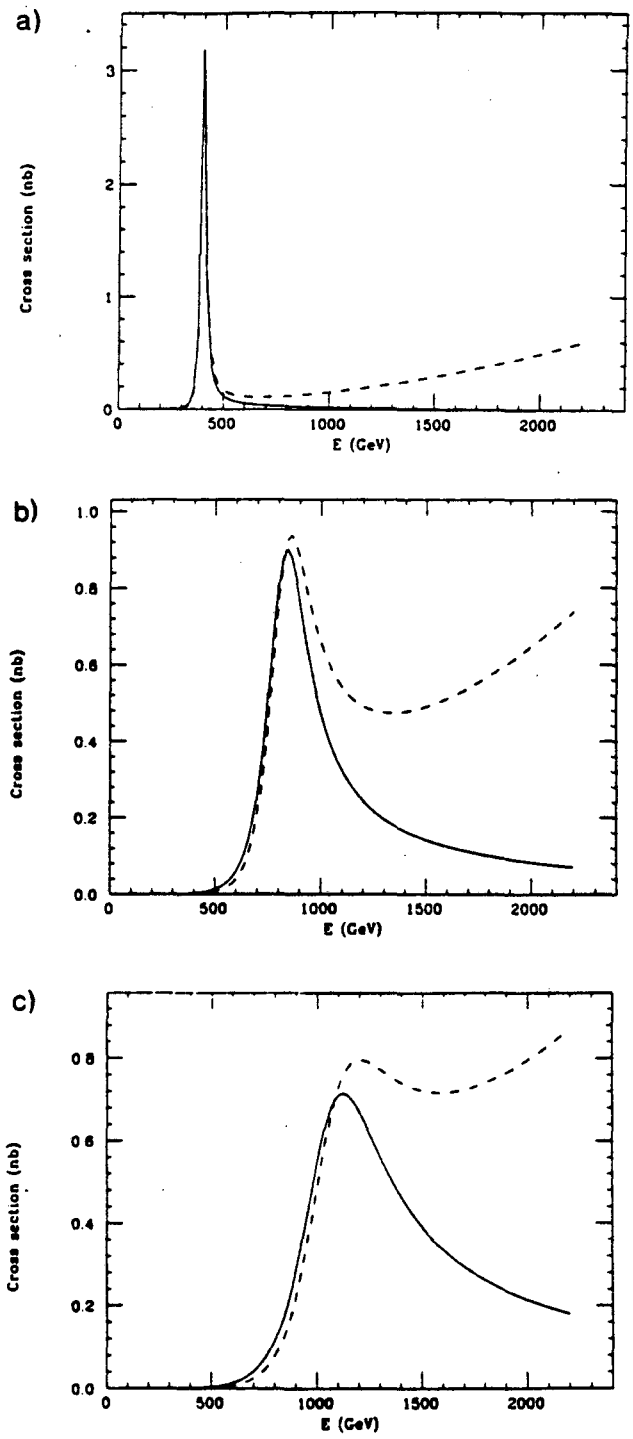


4.1 a) Higgs production via $s$ ,$t$ and $u$ channel diagrams (solid line) and $s$ channel only for $M_H = 400$ GeV. b) Higgs production via $s$ ,$t$ and $u$ channel diagrams (solid line) and $s$ channel only for $M_H = 800$ GeV. c) Higgs production via $s$ ,$t$ and $u$ channel diagrams (solid line) and $s$ channel only for $M_H = 1000$ GeV.

Higgs may be exchanged in the $s$, $t$, and $u$ channels. The solid line plots the correct answer, using all three diagrams. The dashed line shows the effect of leaving out the $t$ and $u$ channel diagrams. At large $ZZ$ invariant mass, the dashed line grows like $s^2$. In the process $qq \to qqZZ \to qqH \to qqZZ$, these matrix elements will get multiplied by appropriate structure functions, which are rapidly falling functions of diboson mass. The bad high energy behavior of the non-unitary matrix element manifests itself as a long flat tail of events at high diboson mass. This approximation cannot be used for invariant masses above about 1200 GeV, and it cannot be used at all for Higgs masses of 1 TeV or above.

PYTHIA's approximation also neglects low energy scattering of the incoming $V$'s (from the photon exchange, for example), and therefore may underestimate the cross section at $ZZ$ invariant mass below the Higgs peak. This is unimportant in practice.

Figures 4.2a-c show the cross section vs $WW$ invariant mass for $pp \to WW + X$ from $WW$ scattering. The Higgs mass is 800 GeV, and there is a rapidity cut on the outgoing $W$'s $|y_w| < 1.5$. Figure 4.2a is a partonic calculation using the effective-$W$ approximation, including all the diagrams for $V_L V_L \to W_L^+ W_L^-$. Figure 4.2b is the result from ISAJET, and Fig. 4.2c is from PYTHIA. Note that Figs. 4.2a and 4.2b have virtually no events above about 1500 GeV, while Fig. 4.2c has a long tail extending up to high energy. This tail is fictitious, and must be removed by truncating the curve at 1200 GeV. The low energy shapes of 4.2a and 4.2b are also different from Fig. 4.2c. The agreement of Figs. 4.2a and 4.2b does not necessarily indicate that ISAJET's calculation is more correct than PYTHIA's, but only that the approximation used in the parton level program which computed Fig. 4.2a is the same as used by ISAJET.

The features of ISAJET and PYTHIA Higgs production cross-sections were checked against two different parton level programs. The first[28] computes the diagram for $qq \to qqVV \to qqH \to qqZZ$ exactly, without using the effective-$W$ approximation. The second uses the effective-$W$ approximation, including all diagrams for $V_L V_L \to W_L^+ W_L^-$. Of course, these two approaches suffer from the same diseases as PYTHIA and ISAJET, respectively. Therefore a cut at an invariant $ZZ$ mass of 1200 GeV is used with program 1, and some cut away from the photon pole must always be used with program 2.

Program 1 can be used to calculate the transverse momentum of the Higgs. Figures 4.3a-c show cross-section vs. $P_T$ of the Higgs from program 1, ISAJET and PYTHIA, respectively. The Higgs mass is 800 GeV, and a cut on the rapidity of the Higgs of $|y_H| < 1$ was imposed. (These curves are insensitive to both the Higgs mass and the rapidity cut.) These curves show that ISAJET and PYTHIA are in substantial agreement with the parton level calculation.

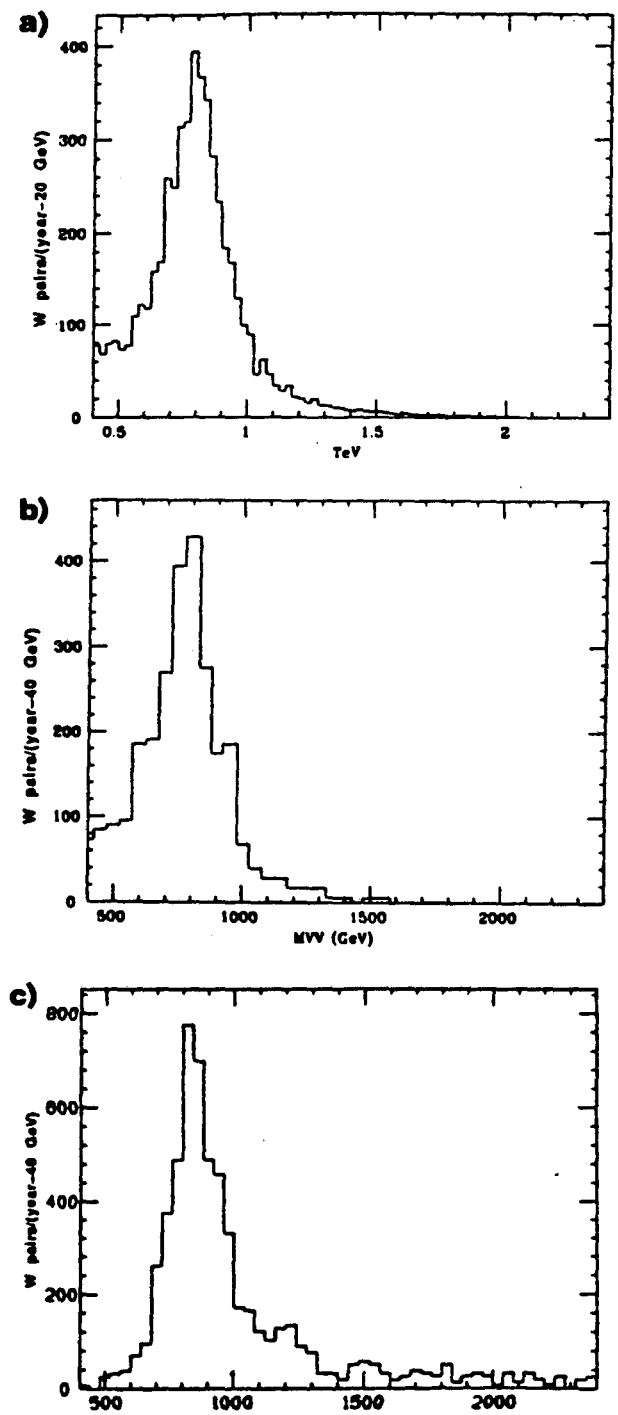


4.2 a) The $WW$ invariant mass distribution in 40 GeV bins from an 800 GeV Higgs resulting from a partonic calculation using the effective $W$ approximation. A cut of $|y_W| < 1.5$ is applied. b) The $WW$ invariant mass distribution from ISAJET for $M_H = 800$ GeV and $|y_W| < 1.5$. c) The $WW$ invariant mass distribution from PYTHIA for $M_H = 800$ GeV and $|y_W| < 1.5$.

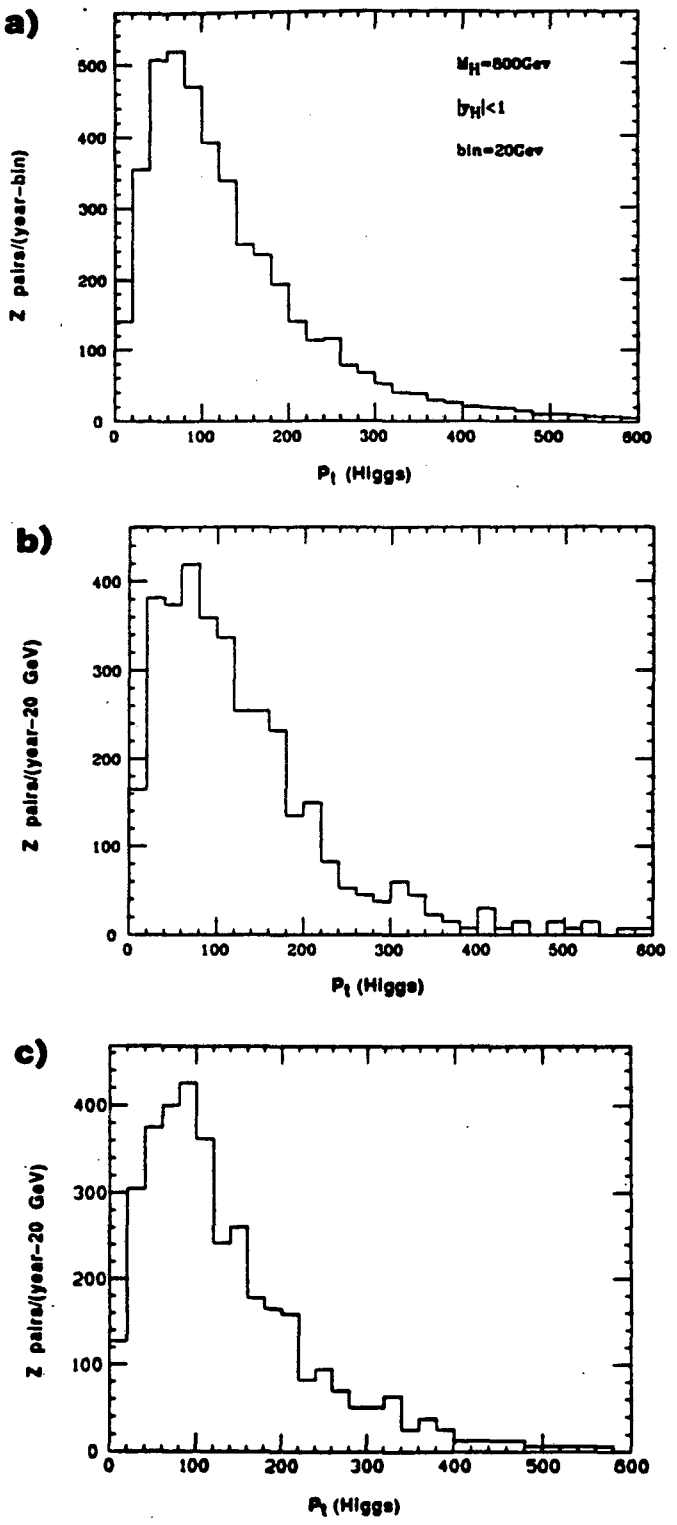


4.3 a) The $P_T$ distribution of an 800 GeV Higgs as calculated by the parton-level program of Cahn et al. We required $|y_H| < 1$. b) The $P_T$ distribution of an 800 GeV Higgs as calculated by ISAJET. c) The $P_T$ distribution of an 800 GeV Higgs as calculated by PYTHIA.

Table 4.2 shows the comparison of the total rates from ISAJET, PYTHIA, and the two parton level programs. Parton program 1 was used to calculate the ZZ rates in the "Partonic" column, while program 2 was used to compute the WW rates.

From this table it is not entirely clear that the normalizations of ISAJET and PYTHIA agree with those in the parton computations. One would expect that ISAJET's WW rates would agree very closely with the parton WW column, since the same approximation was used to compute these two values. One might anticipate that ISAJET would predict a slightly higher rate for WW than the parton calculation, since it includes the transversely polarized outgoing $W$'s. However, this difference should vanish at large Higgs mass, as the signal becomes virtually all longitudinal.

However, none of the numbers differ from the "Partonic" column by more than about 25%, so both ISAJET and PYTHIA may be used for the purposes of this workshop, especially since there is an ambiguity of approximately the same size depending on the choice of structure functions.

### 4.2 Backgrounds

ISAJET and PYTHIA also compute backgrounds to Higgs production. The QCD backgrounds are $q\bar{q} \to Z$+jets and $q\bar{q} \to W$+jets. There is also a significant background from continuum production of gauge boson pairs.

The QCD background processes $q\bar{q} \to Zg$, $gq \to Zq$, etc., with $Z \to e^+e^-$ only, were checked by comparing ISAJET and PYTHIA to a partonic calculation. Cutting on $P_T(Z) > 350$ GeV, ISAJET and PYTHIA give 18270 and 18700 events/year respectively. The parton calculation yields 16000.

Checking the continuum production of gauge boson pairs is made simpler by the fact that the matrix elements can be evaluated in closed form.[20,21] Comparison among ISAJET, PYTHIA and Ref. 23 (EHLQ) is complicated by their use of different values for the constants, $Q^2$ scale and structure functions. The situation is summarized in Table 4.3. The choice of $\alpha_{EM} = 1/137$ is probably inferior to 1/128. The choice of $\hat{s}$ for the scale is probably not as good as the scales used by ISAJET and PYTHIA, at least for Z pair production, because it does not represent as closely the extent to which the quark in the $t$-channel diagrams is off mass shell. Note, however, that the only substantial difference between ISAJET and PYTHIA is the $Q^2$ scale.

To test the continuum production of gauge boson pairs by ISAJET and PYTHIA, a program was written that calculates these processes at the parton level. Table 4.4 shows that the results of the partonic calculations depend strongly on which set of parameters is selected from Table 4.3.

**Table 4.2**

Verification of the Higgs Signal from $VV$ Fusion. Events per SSC year are shown. The numbers shown have statistical errors of approximately 5%.

| | ISAJET | PYTHIA | PARTONIC | |
|---|---|---|---|---|
| Case I: $P_T(V) > 50$ GeV, no $y_V$ cut. | | | | |
| $M_H = 800$ GeV | | | | |
| $WW$ | 13400 | 9000 | 12700 | |
| $ZZ$ | 5600 | 4900 | 5400 | |
| Case II: No $P_T(V)$ cut, $\mid y_V \mid < 1.5$ | | | | |
| $M_H = 400$ GeV | | | | |
| $WW$ | 14000 | 15800 | 12400 | $M_{VV} > 350$ GeV |
| $ZZ$ | 6000 | 8000 | 7100 | |
| $M_H = 600$ GeV | | | | |
| $WW$ | 9200 | 8600 | 7400 | $M_{VV} > 400$ GeV |
| $ZZ$ | 3700 | 4100 | 3400 | |
| $M_H = 800$ GeV | | | | |
| $WW$ | 5900 | 4400 | 4800 | $M_{VV} > 400$ GeV |
| $ZZ$ | 2300 | 2300 | 2300 | |

*NB*: The "Partonic" column is from two different programs; *WW*: from the effective $W$ calculation; *ZZ*: from the program of Cahn, Ellis, Kleiss, and Stirling.[28]

**Table 4.3**

Constants used in $q\bar{q} \to VV$

| | ISAJET | PYTHIA | EHLQ |
|---|---|---|---|
| $M_W$ | 83.38 GeV | 83.0 GeV | 83.0 GeV |
| $M_Z$ | 94.11 GeV | 94.0 GeV | 92.0 GeV |
| $\sin^2\theta_W$ | 0.215 | 0.215 | 0.220 |
| $\alpha_{EM}$ | 1/137 | 1/137 | 1/128 |
| Struct fcns | EHLQ I | EHLQ I | EHLQ II |
| $Q^2$ | $\frac{2\hat{s}\hat{t}\hat{u}}{\hat{s}^2+\hat{t}^2+\hat{u}^2}$ | $\frac{1}{2}(p_{1\perp}^2 + p_{2\perp}^2 + m_1^2 + m_2^2)$ | $\hat{s}$ |

**Table 4.4**

Case I: 200 GeV $< P_T <$ 600 GeV, No $y_V$ cut

| | ISAJET Parameters | PYTHIA Parameters | EHLQ Parameters |
|---|---|---|---|
| *WW* | 30800 / 30500 | 20600 / 30200 | 38800 |
| *ZZ* | 6400 / 6700 | 4500 / 6600 | 8500 |

Case II: No $P_T$ cut, $| y_V | < 1.5$ (both bosons)

| | ISAJET Parameters | PYTHIA Parameters | EHLQ Parameters |
|---|---|---|---|
| *WW* | 391000 / 306000 | 304000 / 344000 | 519000 |
| *ZZ* | 70000 / 59000 | 56000 / 65000 | 100000 |

Case III: No $P_T$ cut, $| y_V | < 1.5$ (both bosons), $M_{VV} > 300$ GeV

| | ISAJET Parameters | PYTHIA Parameters | EHLQ Parameters |
|---|---|---|---|
| *ZZ* | 16000 / 15700 | 14000 / 16300 | 22500 |

**Note**: The number of events for *WW* and *ZZ* production per SSC year. In the ISAJET and PYTHIA columns, two numbers are given. The first number is the actual value given by the programs using their default parameters. The second is the value that the parton (EHLQ) program gives using the default parameters of ISAJET and PYTHIA. The numbers shown have statistical errors of about 5%.

About half of the difference between the results with EHLQ parameters and the other two partonic calculations is due to the different $Q^2$. This indicates the need for the higher order calculation of these processes, since only the next order computation can resolve the differences.

Table 4.4 also shows how well ISAJET and PYTHIA agree with the parton computation. ISAJET (v5.34) was exactly a factor of 2 too large for the ZZ rates, due to a mistake in matrix element; this has been corrected in v5.35. This factor of 2 was removed in Table 4.4. Aside from this, ISAJET's numbers appear to be somewhat too large near threshold, but a cut on the invariant mass of the gauge

bosons (as is likely to be made in practice, if the Higgs is substantially heavier than $2M_Z$) removes this excess of events. PYTHIA appears to be substantially below the predictions of the parton program, especially when the cut forces the gauge bosons out to large $P_T$. Therefore, the $q\bar{q} \to VV$ rates from PYTHIA were multiplied by a factor of 1.8 for the analyses described in subsequent sections.

The partonic cross section for the process $gg \to ZZ$ has not been given explicitly.[22] Consequently, the process cannot be incorporated into PYTHIA or ISAJET. Dicus et al.[22] give figures showing the ratio of the $ZZ$ production at the SSC via $gg$ and $q\bar{q}$ annihilation for various kinematic cuts. We shall use these results to estimate the effect of the $gg \to ZZ$ background process.

### 4.3 Conclusions

Theoretical uncertainties in the Higgs production signal are at present quite substantial, and the potential errors in ISAJET's and PYTHIA's calculations are small compared to them. We conclude that

- ISAJET and PYTHIA agree on the background $Z$ + jets.
- ISAJET's $q\bar{q} \to VV$ rates may be high near threshold, but this is irrelevant for studies of a Higgs heavier than about 300 GeV.
- PYTHIA's $q\bar{q} \to VV$ rates are too low. **Rates from PYTHIA are multiplied by a factor of 1.8 for the results described in subsequent sections.**

## 5. Heavy Higgs Decay into All Charged Leptons

The decay of the heavy Higgs into $ZZ$ where both $Z \to ee$ or $\mu\mu$ is the cleanest signature for a heavy Higgs at the SSC. The total Higgs production cross section depends on the $t$-quark mass, as previously noted in Section 3. For all $M_H > 300$ GeV, the branching ratio[31] for $H \to ZZ$ is approximately 30% but depends slightly on the $t$-quark mass. In most of our studies we have assumed a $t$-quark mass of 40 GeV.

Using PYTHIA and $m_t = 40$ GeV, we have generated Higgs events at Higgs masses of 400, 600 and 800 GeV and the continuum $ZZ$ background (increased by the factor of 1.8 as described in Section 4) for an integrated luminosity of $10^{40}$ with $|y_z| < 1.5$ and perfect $e$ and $\mu$ detection efficiency and energy resolution. The results are shown in Figs. 5.1a–c. The curves are simple polynomial and Breit-Wigner fits to the background and signal, respectively. With these assumptions, a Higgs of mass $\approx 600$ GeV could be detected in this mode; above this mass the signal becomes too small and too broad to observe as a bump on top

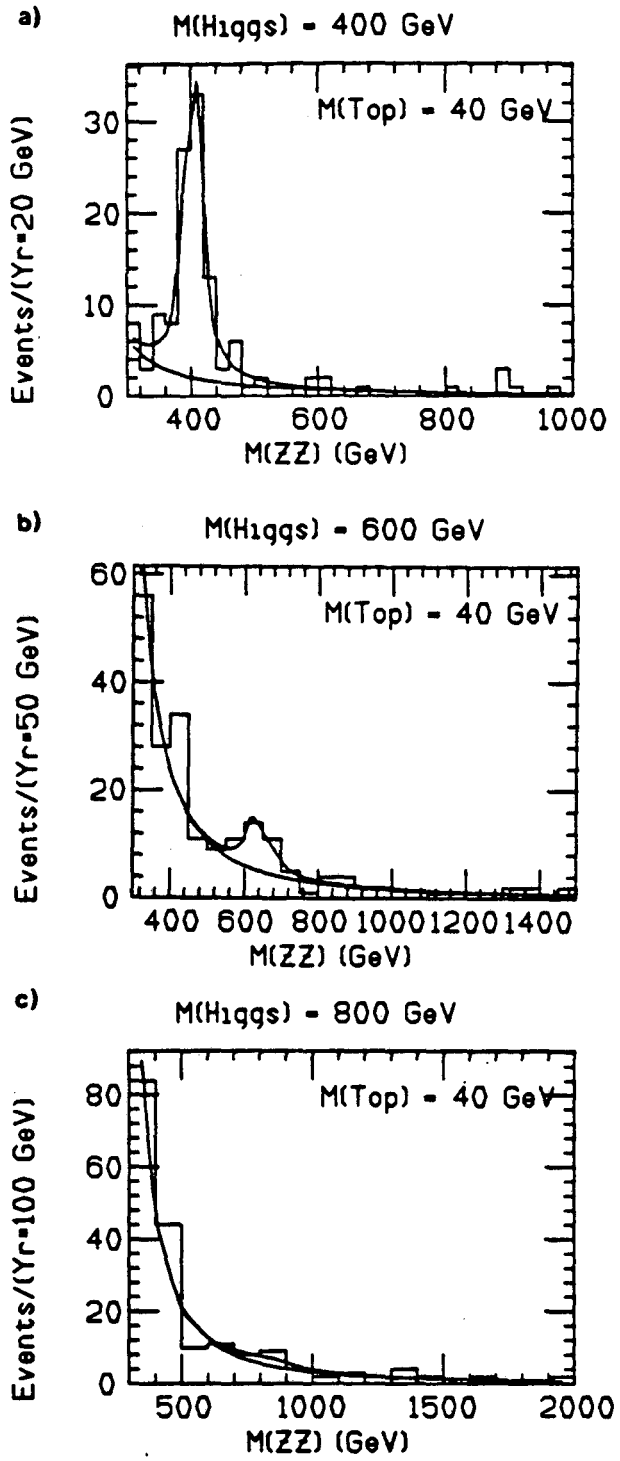


5.1 The $ZZ$ invariant mass distribution arising from Higgs decay and from the background process $q\bar{q} \to ZZ$. The cuts are described in the text. The distribution is shown for Higgs masses of 400, 600, and 800 GeV. If the background process $gg \to ZZ$ were to be included, the background would be increased by a factor which is about 1.7 (1.6) for $M_{ZZ} =$ 400(800) GeV.

of a smooth background. For a top quark mass of ≈40 GeV, it may be possible to discover the Higgs for masses somewhat above 600 GeV *if* both the shape and magnitude of the $ZZ$ background can be determined by calculations together with other measurements which determine the structure functions in the relevant kinematic region.

If the top quark mass is larger, for example 200 GeV, the Higgs signal grows appreciably—see Fig. 5.2a,b and c—in which case discovery of a Higgs in this mode up to ≈800 GeV may be possible. Obviously the mass reach may also be extended by increasing the integrated luminosity. Since this signal at high mass, even with electrons in the final state, appears to be robust (see Section 8.1.4), increasing the peak luminosity rather than the integration time would be desirable.

The $Z$'s from Higgs decay for large $M_H$ are essentially completely longitudinally polarized whereas those from continuum production are not. The use of this polarization information, the decay angular distribution of the leptons in the $Z$ rest frame, can slightly improve the signal to background ratio, by about one standard deviation at 600 GeV. This has been studied in some detail in Ref. 31.

We have also explored the energy dependence of the Higgs production cross section times branching ratio in this mode for a 400 GeV mass Higgs using PYTHIA (for $m_t = 40$ GeV) as described previously. The result of varying the center-of-mass energy from about 11 TeV (≈ today's magnets in the LEP tunnel) to the SSC energy is shown in Fig. 5.3a–d. Studies[32] for the LHC (design energy ≈17 TeV) have shown that 300 GeV is the upper limit in this mode for an integrated luminosity of $10^{40}$, in agreement with the results presented in Fig. 5.3b. Both the signal rate *and* the signal to background improve as the center-of-mass energy is increased—see Fig. 5.4.

From our studies of Higgs $\rightarrow ZZ$, both $ZZ \rightarrow ee$ or $\mu\mu$, we conclude that:

- At the SSC, the Higgs may be discovered in this mode for an integrated luminosity of $10^{40}$ up to a Higgs mass of ≈600 GeV for a top quark mass of ≈40 GeV and up to ≈800 GeV for a top quark mass of ≈200 GeV. This assumes the ability to detect both electrons and muons from the $Z$ decays assuming $|y_z| < 1.5$. Discovery at the upper Higgs mass range limit will likely require quantitative knowledge of the $ZZ$ continuum background shape and magnitude rather than simple "bump hunting".
- The use of polarization knowledge of the $Z$ decays will help only slightly to discover the Higgs in this mode although it would provide confirmation of the nature of a resonance discovered in the ZZ channel.
- Both the Higgs cross section and ratio of Higgs production to continuum $ZZ$ production depend strongly on the available center of mass energy.

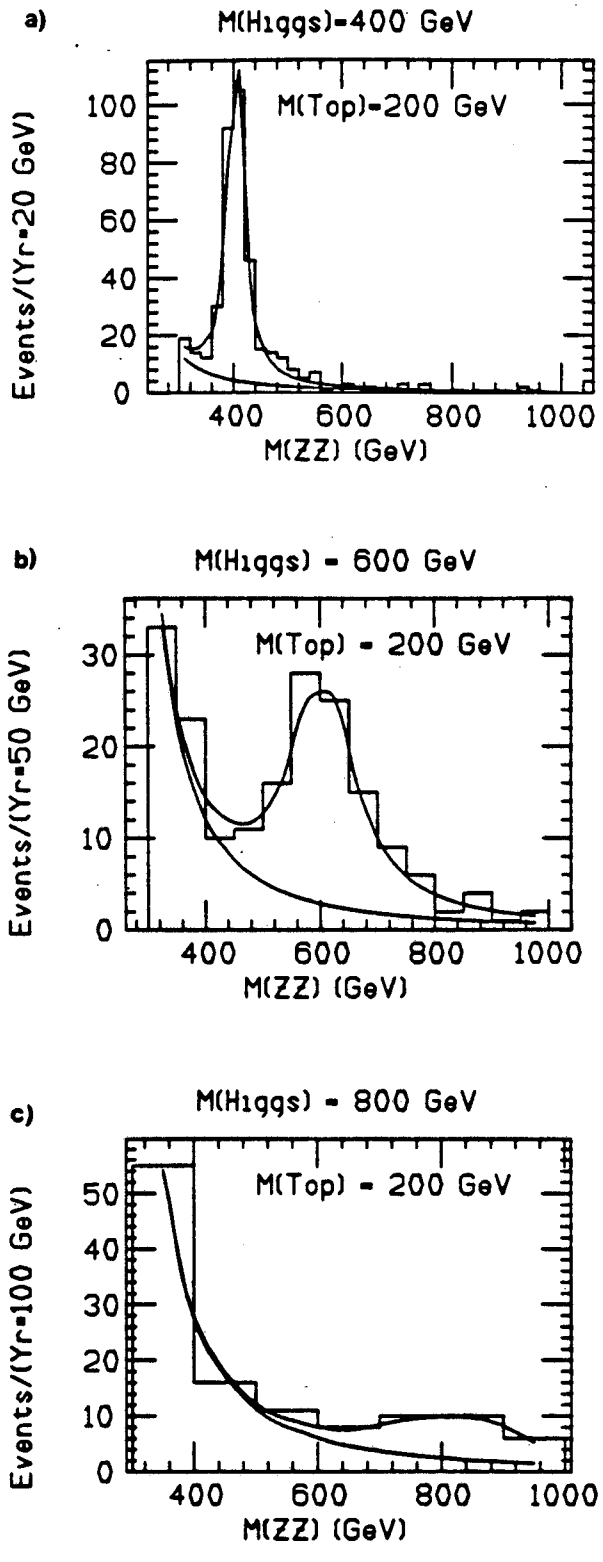


5.2 Same as Fig. 5.1 but for a top quark mass of 200 GeV.

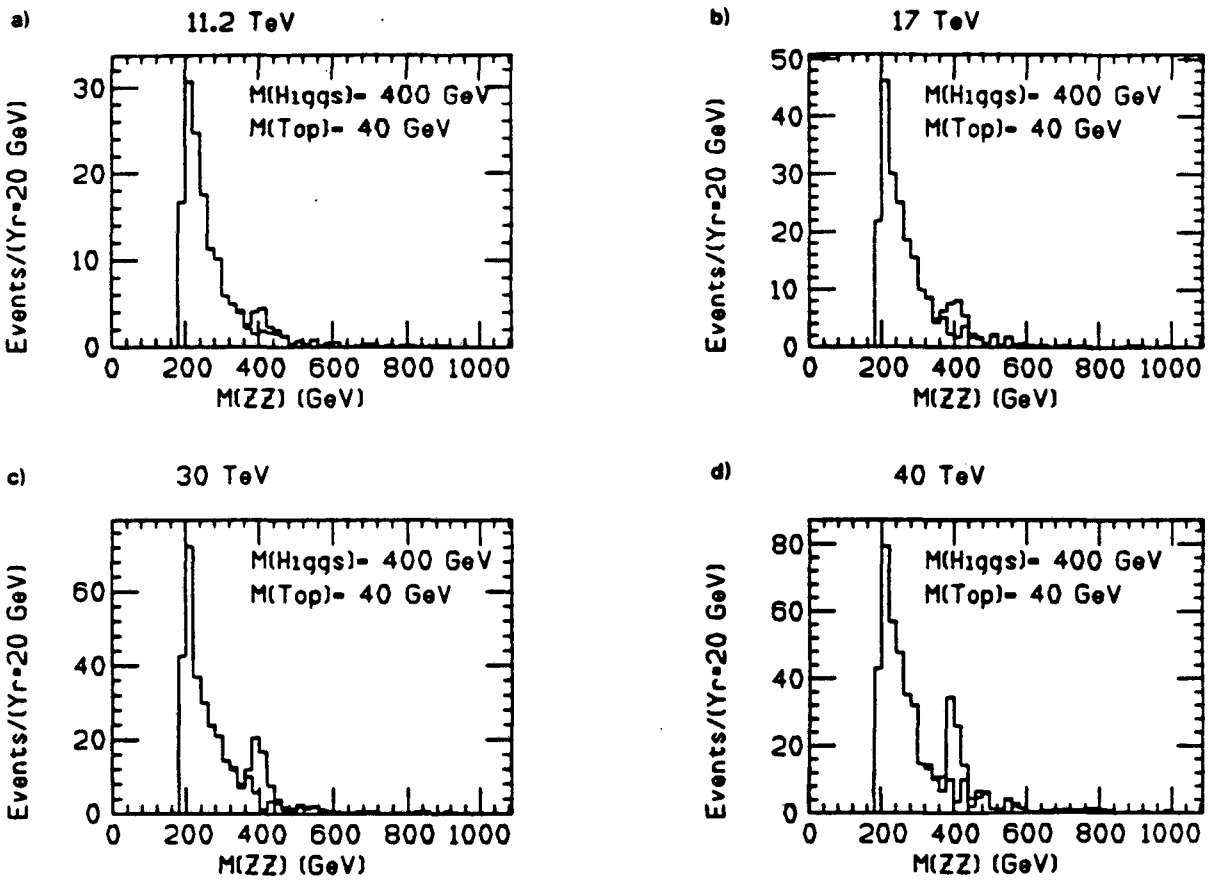


5.3 The center-of-mass energy dependence of Higgs production for $M_H = 400$ GeV for the energies shown.

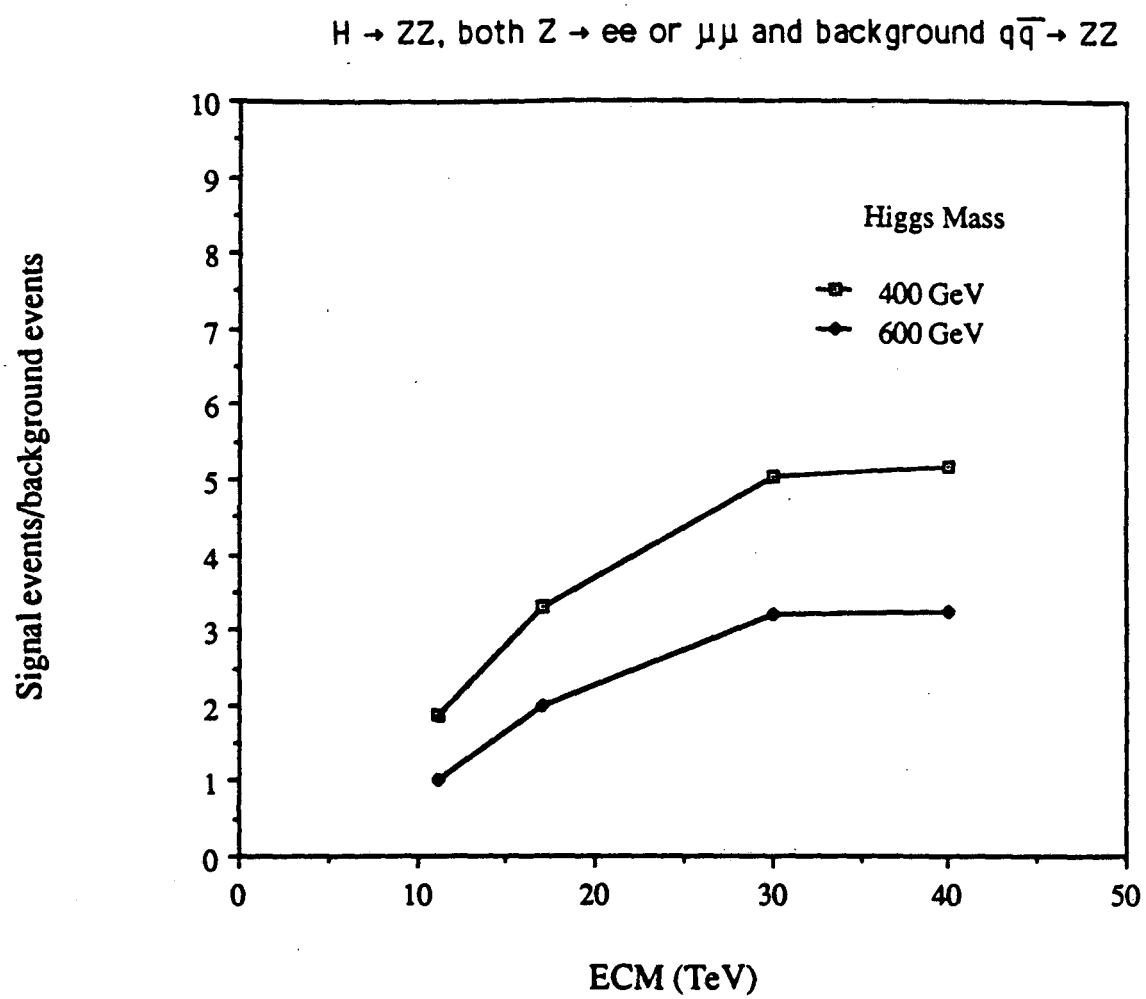


5.4 Ratio of signal events (Higgs) to background events ($q\bar{q}$ production) vs center-of-mass energy for $m_t = 40$ GeV. The $gg \rightarrow ZZ$ background has not been included and would reduce this ratio by 60%.

## 6. Heavy Higgs Decay into Z → *ee* or $\mu\mu$ and Z → $\nu\bar{\nu}$

The advantage of this mode is that the branching ratio is a factor of six larger than the all charged lepton mode. The disadvantage is that single $Z$ + jet(s) production becomes a serious background because its rate is much larger than the Higgs production rate. To remove this background it is important to reject events in which jet activity balances the transverse momentum of the observed $Z \rightarrow ee$ or $\mu\mu$.

It may be possible to tag the quarks recoiling against the gauge bosons that interact to form the Higgs. As shown in Fig. 4.3, the Higgs typically carries about 100 GeV of transverse momentum. This is balanced by the two quark jets, which

are typically at large rapidities. By identifying these jets, it may be possible to reduce some of the backgrounds, especially $q\bar{q} \to ZZ$, which has no such jets. This procedure has been discussed by Cahn et al.,[28] and Barger et al.[33] Tagging has more recently been studied, in the context of the $H \to W^+W^-$ mode, by Kleiss and Stirling (see Section 7).[34] We have little to add on this subject, except to point out that for Higgs masses in the range of interest for this mode, event rates are low and tagging must be done with near perfect efficiency to be useful. There are also likely to be formidable problems in finding jets in the rapidity range 3 to 5 which is required for good tagging efficiency. For purposes of this work, we have not made the assumption that the tagging can be used.

In our analysis, we have focused on Higgs masses above the range accessible via the all charged lepton mode described in Section 5, i.e. for masses greater than ≈600–700 GeV. To be specific we have analyzed the case for $M_H = 800$ GeV. Using ISAJET, we generated Higgs events for $M_H = 800$ GeV and $Z$ + jet(s) events requiring $|y_z| < 1.5$ and $P_T(Z) > 350$ GeV. In both cases the $Z$ decays to either $ee$ or $\mu\mu$. Although other variables may be used,[33] we choose to use the simple transverse mass defined as in the original calculation of Cahn and Chanowitz[44]

$$M_T = 2\sqrt{P_T^2(Z) + M_Z^2}$$

Assuming an integrated luminosity of $10^{40}$, the transverse mass distribution for the Higgs decay and for the background is shown in Fig. 6.1; without additional cuts the background is more than 100 times larger than the signal.

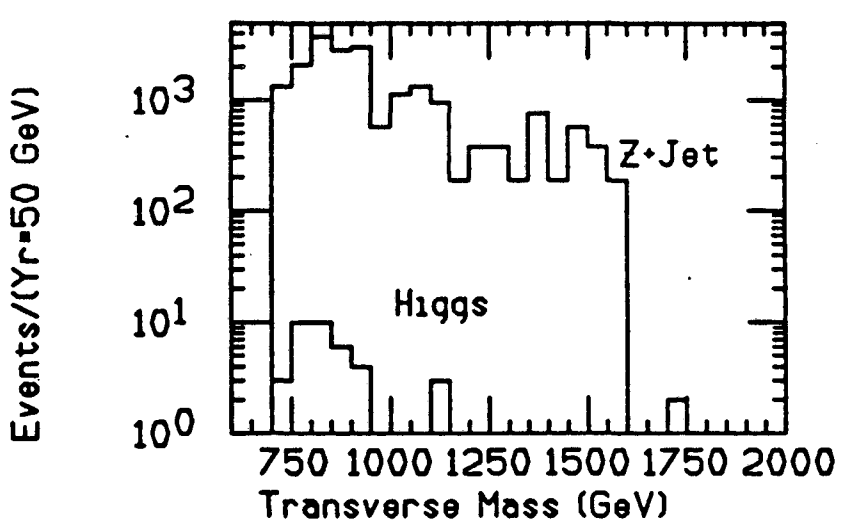


6.1 The transverse mass distribution for Higgs events and for the Z+jet(s) background without cuts on jet activity.

There are a number of ways to quantify and characterize the missing energy signal—see the contribution of A. Savoy-Navarro to these Proceedings,[35] Barger et al.[33] and previous work.[12,36] We have chosen a very simple method to explore the consequences of the lack of detector hermeticity on the background level. First, we assume a quasi-ideal detector with perfect energy resolution, no cracks and a beam hole of $|y| > 5.5$ i.e., particles with rapidity greater than $|5.5|$ are not detected. In the transverse plane of the event (see Fig. 6.2), the total scalar $P_T$ in the half plane opposite to the direction of the $Z$

$$P_T^{back} \equiv \sum_{back-half\ plane} |\vec{P}_T|$$

is computed. For Higgs events this should be small since the only jet activity is from the recoil quarks and beam remnants. For the $Z$ + jet(s) background this should be larger since there will be at least one jet in the event, roughly opposed to the $Z$. The distribution of $P_T^{back}$ for signal and background is shown in Fig. 6.3a. Under these quasi-ideal assumptions, the $Z$ + jet(s) background can be completely eliminated by cutting on $P_T^{back}$, at least within the statistics of our background simulation. The remaining background will then be true $ZZ$ continuum production which has a $P_T^{back}$ distribution similar to that of the Higgs.

Clearly as one degrades the hermeticity of the detector, this clean separation is likely to be diminished. We have explored the consequences of

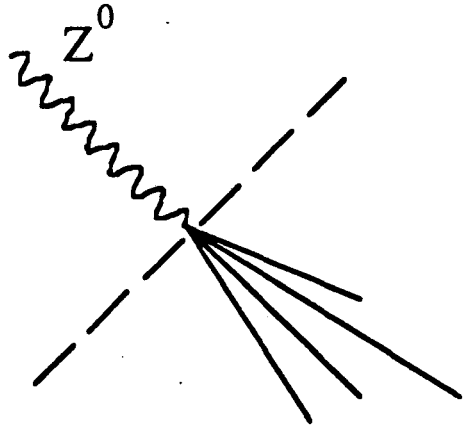


$$P_T^{back} = \sum_{\text{back half plane}} |\vec{P}_T|$$

6.2 Definition of $P_T^{back}$ which is a simple characterization of jet activity.

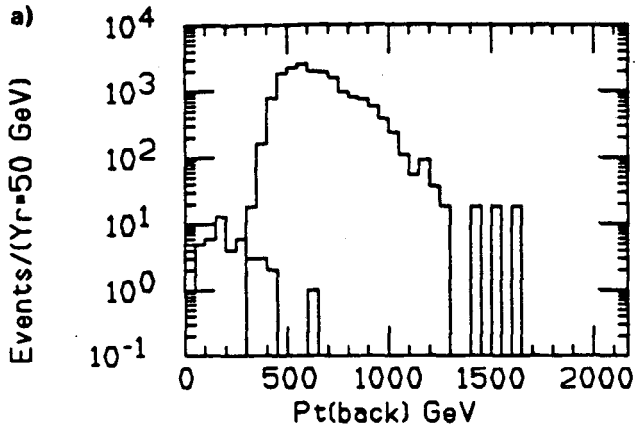


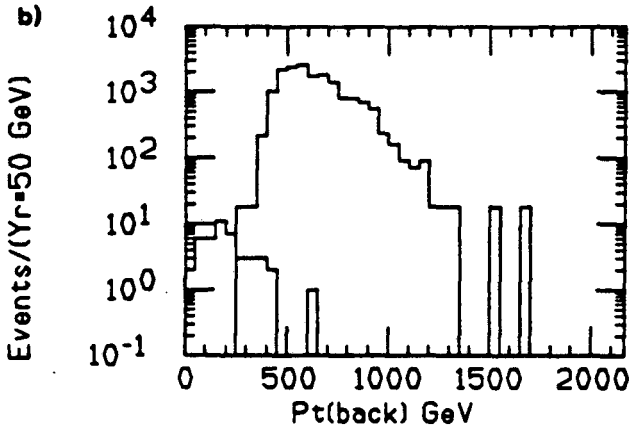


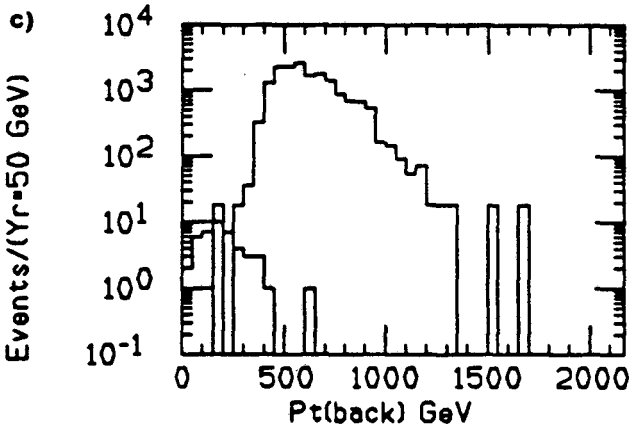


6.3 a) Distribution of $P_T{}^{back}$ for a hermetic detector (for $|y| < 5.5$) with perfect efficiency and energy resolution.
b) Same as (a) but including calorimeter energy resolution and granularity as described in the text.
c) Same as (b) but 2% of the calorimeter cells are dead, which crudely simulates cracks.

- including calorimeter (Gaussian) energy resolution (EM: 15% / $\sqrt{E}$, HAD: 40%/$\sqrt{E}$) and granularity ($\Delta\phi = \Delta y = 0.05$) (Fig. 6.3b) and
- simulating "cracks" by assuming a random 2% inactive cells in the calorimeter (Fig. 6.3c) in addition to energy resolution and granularity

Including energy resolution and granularity effects shifts the lower edge of the distribution of $P_T^{back}$ for the background to lower values. In our simple model of cracks, again some energy is lost in an occasional background event, worsening the separation between signal and background. As the beam hole is enlarged, a similar effect will also occur. Presumably a non-Gaussian calorimetry response would also have such an effect although we have not yet studied this in quantitative detail.

As noted above, assuming a hermetic detector, it is possible to obtain results qualitatively similar to our analysis using different variables as measures of jet activity. In short, independent analyses have shown that given excellent hermeticity and a well understood calorimeter response, the $Z$ + jet(s) background (as presently simulated in Monte Carlo programs) may be reduced to a negligible level. The remaining background, continuum production of $ZZ$ pairs, cannot be easily reduced by these methods. Using our cuts (not optimized) one would therefore obtain a transverse mass distribution (for an integrated luminosity of $10^{40}$) as shown in Fig. 6.4. Since an 800 GeV Higgs is very broad, it is *essential* to know the shape and magnitude of the $ZZ$ background to better than 30%, in

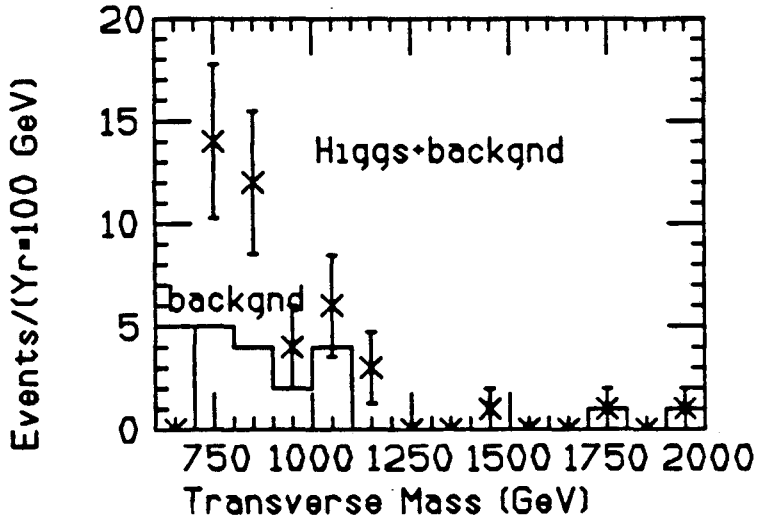


6.4 The transverse mass distribution for $M_H = 800$ GeV after applying cuts which eliminates all the $Z$ +jet(s) background. The remaining background shown arises only from $q\bar{q} \to ZZ$. If the process $gg \to ZZ$ were included, the background would increase by about 60%.

order to exploit this decay mode.† A more realistic detector simulation must be done in order before a definitive statement about the utility of this mode can be made.

## 7. Heavy Higgs Decay into $WW$, $W \to e\nu$ or $\mu\nu$ and $W \to q\bar{q}$

The advantage of this mode is that it has a much larger event rate ($B(H \to llll) = 1.4 \times 10^{-3}$ and $B(H \to W^+W^- \to l\nu q\bar{q} = 0.16)$. There is a large background from $W$ + jet(s) production where the jet system has an invariant mass close to the $W$ mass. This rate is substantially larger than the Higgs rate. To separate the Higgs signal from this background, one must be able to distinguish $W \to q\bar{q} \to$ jets from QCD jets of similar invariant mass with rejection factors of the order of 100:1 or more.[37]

Our investigations concerning the observability of this mode are incomplete, and we have very little to add to published studies[36,38] and other contributions to these Proceedings.[35] Detailed studies[12] have shown that, at the parton level, it is possible to reduce the $W$ + jet(s) background to a level comparable to the Higgs signal if the $t$ quark mass is less than the $W$ mass. Savoy-Navarro[35] in her contribution to these Proceedings states that a $5\sigma$ (signal to background of 1:12) effect can be found via a series of cuts, but this analysis neglects the continuum $WW$ production and assumes that the $W$ + jet(s) rate is precisely known.

In a recent LHC study, Kleiss and Stirling[34] have examined the effectiveness of tagging the outgoing quark jets in this mode. They consider the QCD process $qq \to Wjjjj$ as a source of background to tagged gauge boson fusion Higgs production. They impose cuts requiring two jets in the central region ($|y_{jet}| < 2$) which reconstruct to a $W(|M_{jj} - M_W| < 5$ GeV), and two high energy jets in the forward region ($3 < y_{jet} < 5$, and $E_j > 1$ TeV). They find about 43 events in the signal, and about 260 in the background, at $\sqrt{s} = 17$ TeV. They then impose an "asymmetry cut" requiring that the two central jets have energies which are not too different.

$$(E_1 - E_2)/(E_1 + E_2) < 0.5$$

They find about 31 events in the signal, and 35 in the background. It must be noted, however, that their calculation is purely partonic, and therefore it may significantly overestimate the effectiveness of these cuts, especially the asymmetry cut.[35,38] Moreover, their calculation does not include backgrounds from processes like $gg \to WWjj$. Clearly, more work is needed before a definite conclusion can be reached regarding the effectiveness of tagging.

† If the $t$ quark mass is very large, the production rate is enhanced and a greater uncertainty in the background could be tolerated.

If the $t$ quark mass is larger than the $W$ mass, then $t$ quarks will decay into real $W$'s and the $WW$ background will be substantially increased, making it impossible to exploit this mode.[39]

## 8. Detector Requirements

Considerable work remains to be done before the optimal set of criteria for extracting a heavy Higgs signal can be determined. However, the detector parameters required both to observe the heavy Higgs signal in various decay modes and to reduce or eliminate backgrounds can now be reliably estimated. Even though the best set of experimental cuts is not well understood, detector parameters can be specified reasonably well. In the sections below we describe the motivation for the choice of detector parameters for the three decay modes of interest. We also describe the requirements for the observation of gauge boson pair production including the $W^{\pm}W^{\pm}$ and $WZ$ channels.

### 8.1 Heavy Higgs $\rightarrow ZZ$, both $Z \rightarrow ee$ or $\mu\mu$

The parameters of interest include:

- the angular or rapidity acceptance for the leptons
- the transverse and total momentum distribution of the leptons
- the opening angle distribution
- the momentum or energy resolution required
- lepton sign determination
- lepton identification criteria, particularly the jet rejection needed to observe electrons, and
- vertex criteria, both primary and secondary vertices.

In the sections below, each of these items is discussed. A summary is given in Table 8.1.

#### *8.1.1 Rapidity Acceptance*

In order to reduce the background from continuum $ZZ$ production, a cut of $|y_z| < 1.5$ is usually applied,[23] restricting the rapidity range of the leptons from the $Z$ decay. With this cut, the four-lepton acceptance vs. the lepton rapidity coverage is shown in Fig. 8.1 for 400 and 800 GeV Higgs masses. Electron and muon coverage of $|y| < 2.5 - 3$ is adequate.

#### *8.1.2 Transverse and Total Momentum Distribution of the Leptons*

In Figs. 8.2 and 8.3 we plot the $P_t$ distributions of leptons in Higgs events after requiring $|y_z| < 1.5$, for $M_H = 400$ and 800 GeV. The hatched bins in these

**Table 8.1:** Summary of experimental requirements for $H \to ZZ \to \ell^+\ell^-\ell^+\ell^-$. For details see the text.

| | | |
|---|---|---|
| $z$ vertex resolution | | $\approx 1cm$. |
| Secondary vertex | | Not needed. |
| Charged hadron tracking | $y$ coverage | Backup for calorimetry. |
| | Resolution | Not critical. |
| Electron identification | $y$ coverage | $\|y\| \lesssim$ 2.5-3. See Fig. 8.1. |
| | $\Delta E/E$ | $\approx .15/\sqrt{E}$. Must reconstruct $M_Z$ for all $M_H$. |
| | $P_T$ range | $\lesssim M_H$. See Figs. 8.2 and 8.3. |
| | Jet rejection | $Z$ mass constraint adequate for $M_H \gtrsim 500GeV$. Not known for smaller masses. |
| | Charge measurement | Not needed for $M_H \gtrsim 400GeV$. |
| Muon identification | $y$ coverage | $\|y\| \lesssim$ 2.5-3. See Fig. 8.1. |
| | $\Delta p/p$ | $\lesssim 15\%$ if $m_t \lesssim 100GeV$. Better if $m_t$ is larger. |
| Calorimetry | $y$ coverage | Same as for $e^\pm$. |
| | $\Delta E/E$ | See electrons. Not important for hadrons. |
| | Segmentation | $\Delta y = \Delta\phi \approx$ 0.03-0.05. |
| | Hermeticity | Not important. |
| Luminosity | | Need $\mathcal{L} \sim 10^{33}cm^{-2}s^{-1}$. Perhaps can use $\mathcal{L} \sim 10^{34}cm^{-2}s^{-1}$. |
| Trigger | | Require leptons above $P_T \sim 10GeV$. Higher level: make loose cuts on $Z$ mass and $P_T$. |

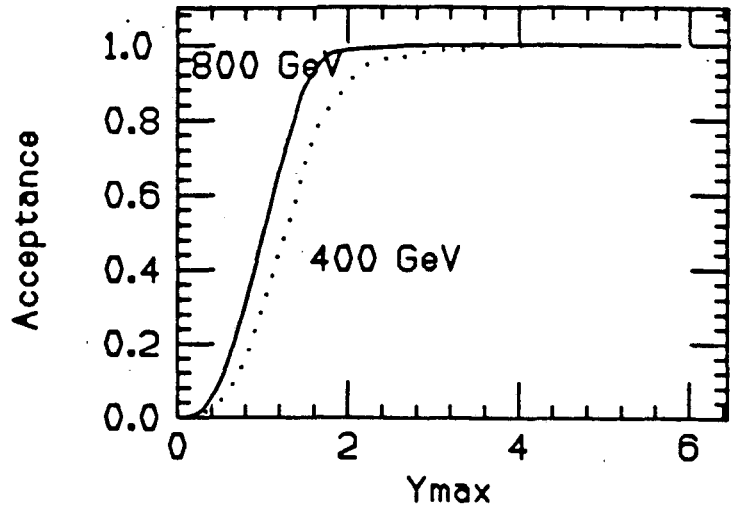


8.1 The four-lepton acceptance vs lepton rapidity coverage.

figures indicate the contributions from leptons in the same events which do not come from the Higgs decay; for example, they are from $\pi^0$ Dalitz decay. This contribution is small and limited to low $P_T$.

By examining the distribution of the lowest $P_T$ lepton from the Higgs decay, we also find that identification of leptons down to $P_T \sim$ 20–50 GeV is required for good efficiency.

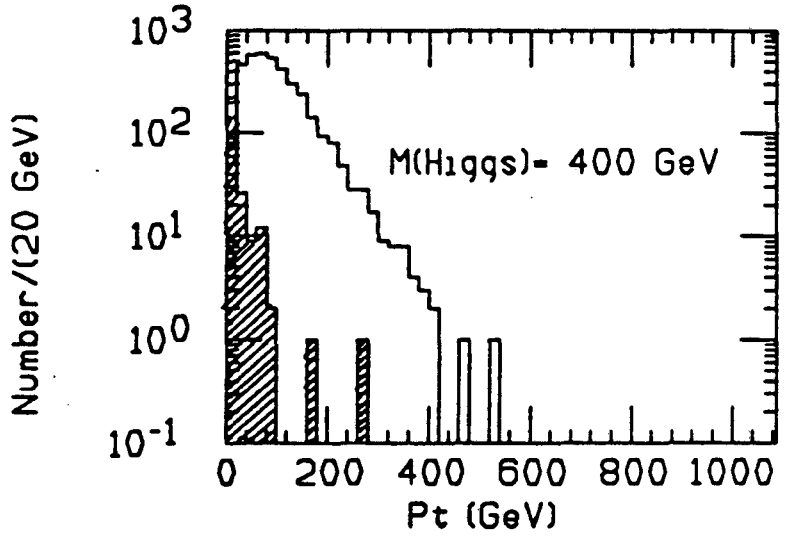


8.2 The $P_T$ distribution of electrons in Higgs events for $M_H$ = 400 GeV. The hatched bins indicate the contribution from non-$Z$ sources in Higgs events.

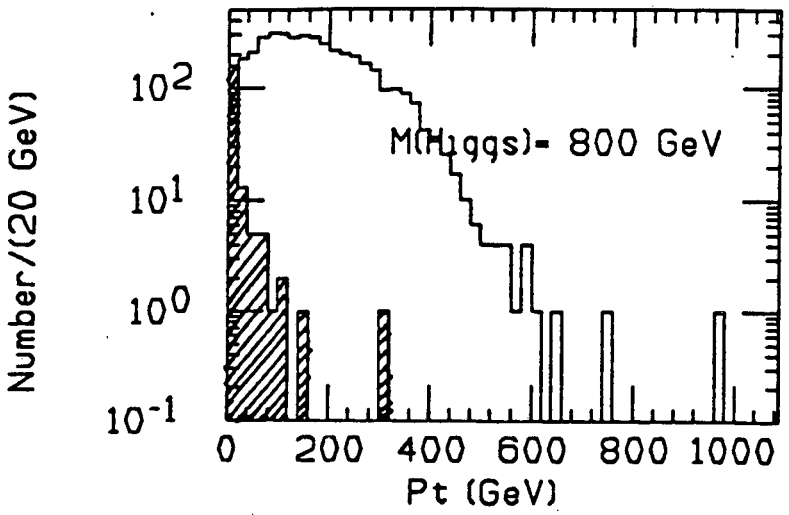


8.3 Same as 8.2 but for $M_H = 800$ GeV.

In Fig. 8.4 we show the four-lepton acceptance vs. total momentum of the most energetic lepton. The acceptance is about 50% for a total momentum of about one-half of the Higgs mass.

*8.1.3 Opening Angle Distribution*

The opening angle distribution between the two leptons from the $Z$ decay is of interest because good angular granularity in a calorimeter is required to separate the two electrons and reconstruct the $Z$ mass. It is also important to

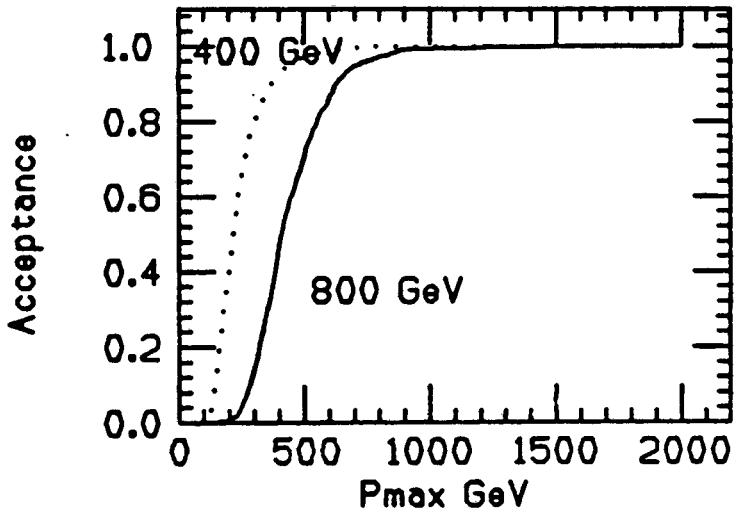


8.4 The four-lepton acceptance vs the total momentum of the most energetic lepton.

have adequate two-track resolution for the muon tracking system. The opening angle distribution for $M_H = 800$ GeV is shown in Fig. 8.5. Note that for such a large Higgs mass, there is a substantial spread of the $ZZ$ invariant mass since the Higgs width is large, so the opening angle distribution is different from that expected for a narrow 800 GeV particle. In order to separate the two electrons with good efficiency and measure their energies, an angular resolution of $\Delta\eta = \Delta\phi \approx 0.03 - 0.05$ is required.

### *8.1.4 Momentum and Energy Resolution and Charge Determination*

The issues here are: (1) do we need to determine the charge of electrons in order to properly reconstruct the $Z$ mass (reduce background)?; and (2) how well must muon or electron momenta be measured to find the $Z$ mass and reduce potential backgrounds? Some aspects of these issues have been studied by Paige[40] and by Chen et al.[41] in contributions to these Proceedings. Definite resolution of these issues is not simple since the results depend on the Higgs mass, the $t$ quark mass and on modeling of jet rejection for identification of electrons or muons.

Paige[40] has shown that, for a Higgs mass of 800 GeV, it is possible to eliminate jet backgrounds which simulate electrons using simple calorimetric and isolation cuts. Electrons from the $Z$'s in Higgs decay have high $P_T$, are isolated and can be paired to form the $Z$ mass; electron candidates from QCD jets do not have these properties. Determination of the electron charge is not required in this analysis. Although this analysis has been done for an 800 GeV Higgs mass, it would likely apply down to Higgs masses in the 500–600 GeV range. For lower masses the jet background, relative to the signal, becomes larger and $P_T$ cuts are less effective.

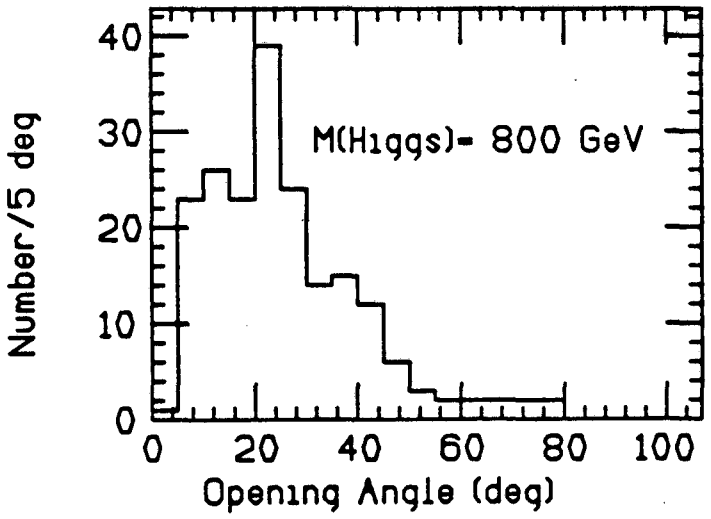


8.5 The opening angle distribution of electrons from $Z \to ee$ for 800 GeV Higgs decays.

Chen et al.[41] have emphasized the need for good momentum resolution to observe the $Z$ mass peak in the presence of a dilepton background resulting from heavy top quark ($m_t$ = 200 GeV) decay. If the $t$ quark is sufficiently massive, there is a copious dilepton background from $t\bar{t} \rightarrow WW + X$ production which populates the invariant mass region in the neighborhood of the $Z$. In their contribution, Chen et al. show that muon momentum resolution characteristic of an iron spectrometer results in a dimuon muon invariant mass distribution in which the $Z$ is barely visible because of the $t\bar{t}$ background.

However, for the all charged lepton mode and for Higgs masses above about 400 GeV, this background can very likely be eliminated by simply cutting on the transverse momenta of the dimuon pairs. To test this hypothesis we generated $t\bar{t}$ events for $m_t$ = 200 GeV and required events with at least two $ee$ or $\mu\mu$ (or the combination) pairs with $|y_{e \text{ or } \mu}| < 3$. In order to increase the stastical power of our estimates, we required $W \rightarrow e\nu$ or $\mu\nu$ and $b$-hadron semileptonic decay. Analysis of a smaller sample of events without this restriction indicates that these decays are the dominant source of $\geq 4$ lepton events. We also require the dilepton mass of both pairs, formed from different leptons, to be between 70 and 110 GeV. In Fig. 8.6 we show a scatter plot of the $P_T$ of one lepton pair vs. the $P_T$ of the other, corresponding approximately to 1/100 of an SSC year. The magnitude of this background is reasonably described by an exponential distribution when plotted against a minimum $P_T$ for both pairs. For example, about 100(10) events/year would remain requiring a minimum $P_T$ of 150(200) GeV. Hence this background should be negligible for masses of the Higgs greater

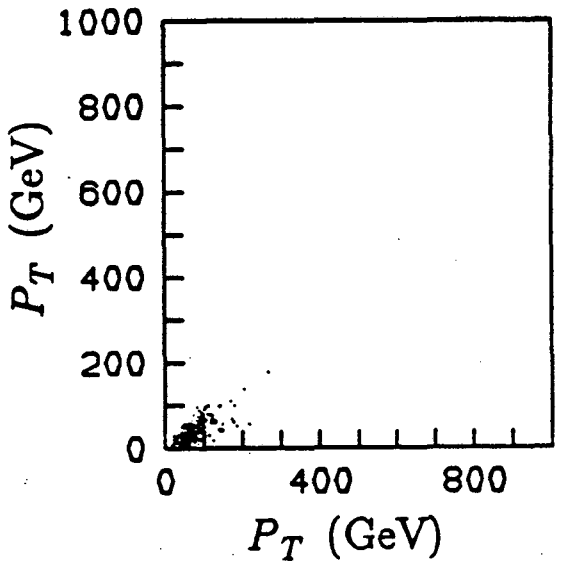


8.6 A scatter plot of $P_T$ of one dilepton pair from $t\bar{t}$ events vs. $P_T$ of the other pair with cuts described in the text.

than about 400 GeV. We note that Chen et al. in their analysis also applied a cut (of 300 GeV) on the $P_T$ of the dimuon pair but some $t\bar{t}$ background remained. Requiring a second $Z$ candidate eliminates the remaining background. Of course, this method only works for the all charged lepton mode of Higgs decay. For the mode with only one $Z$ decay to $ee$ or $\mu\mu$, and $Z \rightarrow \nu\bar{\nu}$ good resolution may be more important. A similar study for this mode has not yet been done.

### *8.1.5 Longitudinal Vertex Resolution*

At the SSC, the rms longitudinal bunch length is expected to be about 7 cm and hence the protons interact in a region about 20 cm long. In a high luminosity environment it may be difficult to determine the precise longitudinal location of the event vertex. For events containing muons, previous studies have shown that it is possible to trace stiff muon trajectories through absorber back to the origin[42] with reasonable accuracy. For electrons this requires central tracking information, which may be unattainable at the highest luminosities.

To estimate the effect of the uncertainty in the longitudinal vertex position, we generated 800 GeV Higgs events decaying into four electrons for different rms beam spot length sizes. The electrons are assumed to be measured with perfect energy and position resolution at a radius of 1 meter. The four highest $P_T$ electrons in the event are selected (these are almost always the electrons from the Higgs). The pair, $M_{12}$, forming an invariant mass closest to the $Z$ is found and the invariant mass of the other pair, $M_{34}$, calculated. This was done for three different assumptions about the accuracy to which the longitudinal vertex position is known—see Fig. 8.7. The $M_{34}$ distribution is significantly broader than the $Z$ intrinsic width if an rms resolution of 7 cm is assumed. Since one will be dealing with small event samples, it would seem prudent to have some means for crude ($\approx 1-2$ cm) measurements of the longitudinal vertex position but millimeter measurements will not be required.

### *8.1.6 Summary of Detector Requirements for this Mode*

In Table 8.1 we summarize the key detector related parameters determined by Higgs $\rightarrow ZZ$, both $Z \rightarrow ee$ or $\mu\mu$. In many cases only qualitative conclusions can be reached at this time. Many of the parameters depend on the Higgs mass and on the $t$ quark mass. More work is required to better quantify some of the requirements.

## 8.2 Higgs Decay to $ZZ$, $Z \rightarrow ee$ or $\mu\mu$ and $Z \rightarrow \nu\bar{\nu}$

The experimental requirements for the $Z \rightarrow ee$ or $\mu\mu$ decay in this mode are obviously very similar to those described above. Dilepton mass resolution may be more important in this mode than in the all charged lepton mode. The $t\bar{t}$ background to this mode for large $m_t$ is not known. Rejection of fake $Z$

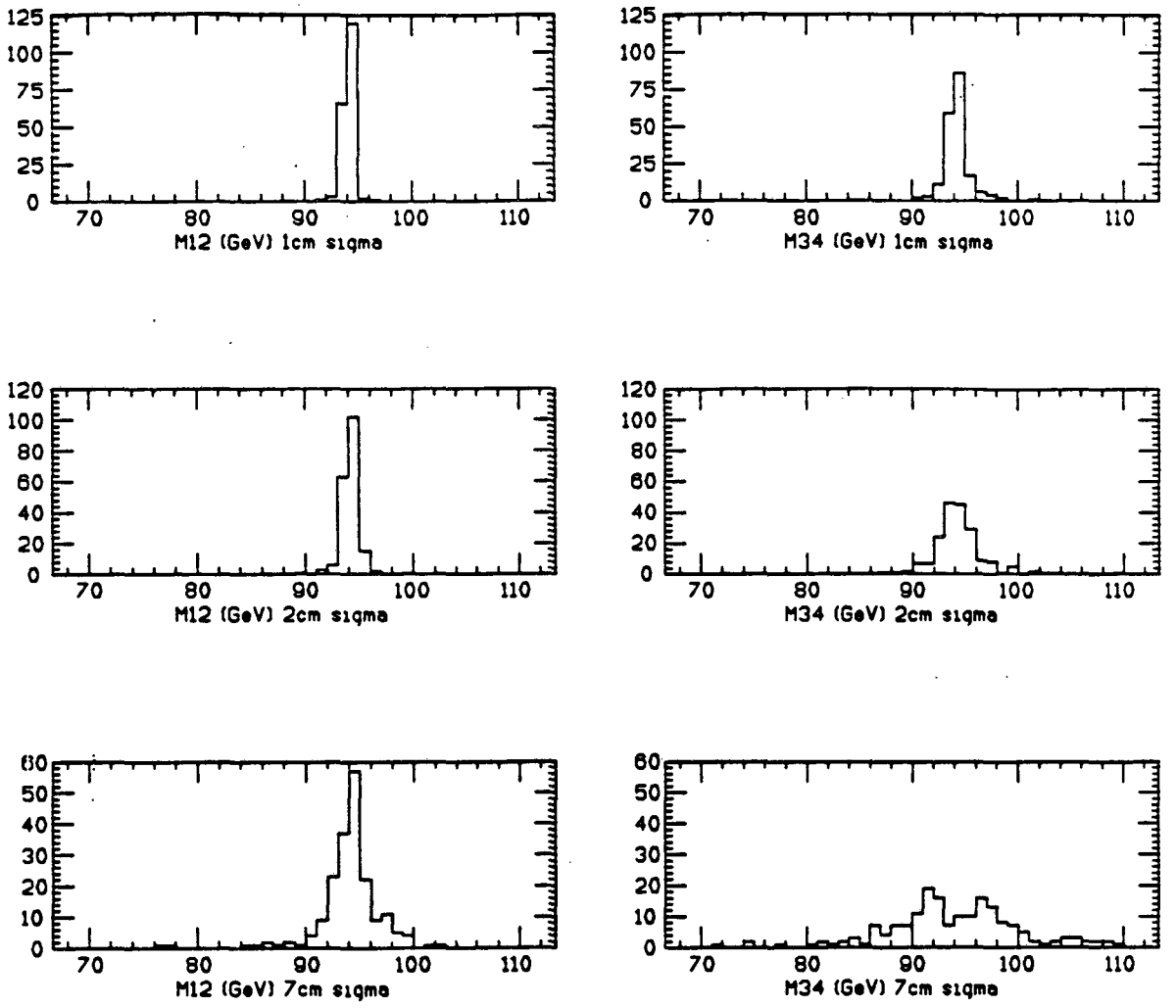


8.7 Dilepton invariant mass distributions $M_{12}$ and $M_{34}$ (see text) for different assumptions regarding the accuracy of determination of the longitudinal vertex of the event.

candidates requires better lepton identification since the event contains one $Z$ and is less constrained. We have not studied this issue in sufficient detail to make a quantitative statement.

Measurement of missing energy is obviously crucial for this mode, We stated in Section 6 that for a hermetic detector, the $Z$ + jet(s) background to this mode, may be completely eliminated with a simple cut on transverse energy recoiling against the $Z$. As the hermeticity is degraded it will become more difficult to eliminate this background. Hence maximum feasible rapidity coverage ($|y| < 5-6$) and minimization of cracks and dead spaces should be the goals for calorimetric coverage. The calorimeter response must also be well understood. In addition, the detection and measurement of muons over a comparable rapidity range would be desirable, since the missing energy background from heavy quark decays and $WZ$ events will be increased if muons are not detected.

We have not explicitly studied the ability to use quark tagging to reduce the $Z$ + jet(s) background. In our simple analysis using transverse energy, explicit jet detection is not required. If jet tagging is to be used, detection of jets in the rapidity range of three to five will be required. Since in any scheme hermeticity is essential, the detector requirements will be similar if transverse energy or jet detection is used. It would be prudent in any case to attempt to detect jets, not just measure energy, over the maximum feasible rapidity range.

The detector parameters required for this mode are summarized in Table 8.2. Additional progress on determining the observability of this mode and the concomitant detector parameters requires a much more detailed simulation of a realistic calorimeter. The observability of a Higgs signal in the mode $Z \to ee$ or $\mu\mu$ and $Z \to \nu\bar{\nu}$ depends strongly upon the details of calorimeter performance.

### 8.3 Higgs Decay to $WW$, $W \to e\nu$ or $\mu\nu$ and $W \to q\bar{q}$

Although it has not been convincingly established, that the Higgs may be discovered via this mode the requisite detector parameters can be determined with some confidence. The dominant background will be $W$ + jet(s) provided the $t$ quark does not decay to $Wb$. If $t \to Wb$ is allowed this mode cannot be utilized.

Rejection of the $W$+jet(s) background requires reconstruction of the $W \to q\bar{q}$ invariant mass with good resolution. This will require fine grained calorimetry with good energy resolution. This has been studied in quantitative detail by Freeman and Newman-Holmes in their contribution to these Proceedings.[43] They find that calorimetric tower sizes of $\approx 0.03$ are required; tower sizes of 0.1 significantly degrade the $W$ mass resolution. Relatively modest energy resolution of $0.15/\sqrt{E}$ for electromagnetic calorimetry and $0.5/\sqrt{E}$ for hadronic is adequate but an electron-to-hadron response near one (within $\pm 0.1$) is very desirable. They also

**Table 8.2:** Summary of experimental requirements for $H \to ZZ \to \ell^+\ell^-\nu\bar{\nu}$. For details see the text.

| | | |
|---|---|---|
| $z$ vertex resolution | | $\approx 1cm$. |
| Secondary vertex | | Not needed. |
| Charged hadron tracking | $y$ coverage | Backup for calorimetry. Important |
| | Resolution | Not critical. |
| Electron identification | $y$ coverage | $\|y\| \lesssim$ 2.5-3. See Fig. 8.1. |
| | $\Delta E/E$ | $\lesssim .15/\sqrt{E}$. Must reconstruct $M_Z$ for all $M_H$. |
| | $P_T$ range | $\lesssim M_H$. See Fig. 8.2, 8.3. |
| | Jet rejection | $Z$ mass constraint adequate for $M_H \gtrsim 500GeV$. Not known for smaller masses. |
| | Charge measurement | Not needed for $M_H \gtrsim 400GeV$. |
| Muon identification | $y$ coverage | $\|y\| \lesssim$ 2.5-3. See Fig. 8.1. |
| | $\Delta p/p$ | $\lesssim 15\%$ if $m_t \lesssim 100GeV$. Better if $m_t$ is large. |
| Calorimetry | $y$ coverage | $\|y\| \leq 5.5$ or better. |
| | $\Delta E/E$ | $0.15/\sqrt{E}$ (electrons), $0.5/\sqrt{E}$ (hadrons). $e/\pi = 1.0 \pm 0.1$. |
| | Segmentation | $\Delta y = \Delta\phi \approx$ 0.03-0.05. |
| | Hermeticity | Crucial |
| Luminosity | | Need $\mathcal{L} \sim 10^{33} cm^{-2}s^{-1}$. Limited by hermeticity requirement. |
| Trigger | | Require leptons above $P_T \sim 10GeV$. Higher level: require loose $Z$ mass and missing $P_T \gtrsim 200GeV$. |

show that the $W$ mass resolution is very sensitive to pile-up of events within the detector resolving time. Low energy particles make a significant contribution to the $W$ mass even for high $P_T$ $W$'s, so the addition of low $P_T$ particles from out-of-time events shifts the reconstructed $W$ mass to higher values. To avoid this problem, calorimetry for $W$ mass reconstruction must be able to time-tag energy deposition. A Monte Carlo study assuming the ability to tag energy deposition but with long integration time should be done.

Calorimetry that is sufficient to permit reconstruction of the $W$ mass should be adequate to allow kinematic cuts on the di-jet system such as those suggested by Gunion.[12] Detection of jets at large rapidity to tag the recoil quarks would have the same requirements and difficulties as discussed in Section 8.2.

The other aspect of this mode is detection of the $W \rightarrow e\nu$ or $\mu\nu$ signal. This requires detection and measurement of single $e$ or $\mu$ over a rapidity and $P_T$ range comparable to that in the other Higgs decay modes. More stringent jet rejection is required since the $Z$ mass constraint is now absent. The required rejection depends on the $P_T$ of the lepton and has not been investigated in detail; we expect a rejection of at least $10^4$ will be required when applied in conjunction with the missing energy signature. A larger rejection may be required at low $P_T$ and a smaller one at high $P_T$. Measurement of missing transverse energy is also required to reconstruct the $W \rightarrow l\nu$ with a zero constraint fit so hermetic calorimetry covering $|y| < 5 - 6$ will be required.

The detector parameters for this mode are summarized in Table 8.3.

### 8.4 Detection of Other Gauge Boson Pairs

In Sections 1 and 3.1 we discussed the motivation for the detection of all gauge boson pairs, not just those arising from Higgs decay. Detection of $W^{\pm}W^{\pm}$ and $WZ$ events is of great importance, since these final states are characteristic of a strongly interacting symmetry breaking sector. Many of the requirements for the detection of same sign $W$ pairs are the same as those for opposite sign pairs, but the charge of the lepton from the $W$ decay(s) must also be determined. Since event rates in the interesting mass region are low, determination of both electron and muon charges is essential.

As discussed in Section 3.2, models for $W^{\pm}W^{\pm}$ or $WZ$ production predict an enhanced rate for these events if there is no Higgs boson of mass less than about 1 TeV. The $P_T$ distribution of the lepton with the largest $P_T$ arising from $W^+W^+ \rightarrow l^+\nu l^+\nu$ is shown in Fig. 8.8. The model of Ref. 4 is used with the requirement that $M_{WW} > 0.5$ TeV and $|y_w| < 1.5$. From this figure, it is clear that one needs to determine the sign of leptons with $P_T < 750 - 1000$ GeV.

**Table 8.3:** Summary of experimental requirements for $H \to W^+W^- \to \ell^\pm \nu q\bar{q}$. For details see the text.

| | | |
|---|---|---|
| $z$ vertex resolution | | Probably not important. |
| Secondary vertex | | Not needed. |
| Charged hadron tracking | $y$ coverage | Backup for calorimetry. If used for $W \to q\bar{q}$ identification, need tracking inside jets. |
| | Resolution | Not critical. |
| Electron identification | $y$ coverage | $\lvert y \rvert \lesssim 2.5$-3. See Fig. 8.1. |
| | $\Delta E/E$ | Not critical. |
| | $P_T$ range | $\lesssim M_H$. See Fig. 8.2, 8.3. |
| | Jet rejection | Required. $e/jet \sim 10^{-4}$. |
| | Charge | Not needed. |
| Muon identification | $y$ coverage | $\lvert y \rvert \lesssim 2.5$-3. See Fig. 8.1. |
| | $\Delta p/p$ | $\lesssim 15\%$ for any $m_t$. |
| Calorimetry | $y$ coverage | $\lvert y \rvert \leq 5.5$ or better to measure $P_T^{miss}$. |
| | $\Delta E/E$ | $0.15\sqrt{E}$ (electrons),<br>$0.5/\sqrt{E}$ (hadrons).<br>$e/\pi = 1.0 \pm 0.1$. |
| | Segmentation | Needed for background rejection.<br>$\Delta y = \Delta\phi \approx 0.03 - 0.05$. |
| | Hermeticity | Needed to see $\nu$. |
| Luminosity | | Need $\mathcal{L} \sim 10^{33} cm^{-2} s^{-1}$.<br>Limited by hermeticity requirement and $W \to q\bar{q}$ reconstruction. |
| Trigger | | Not studied in sufficient detail. |

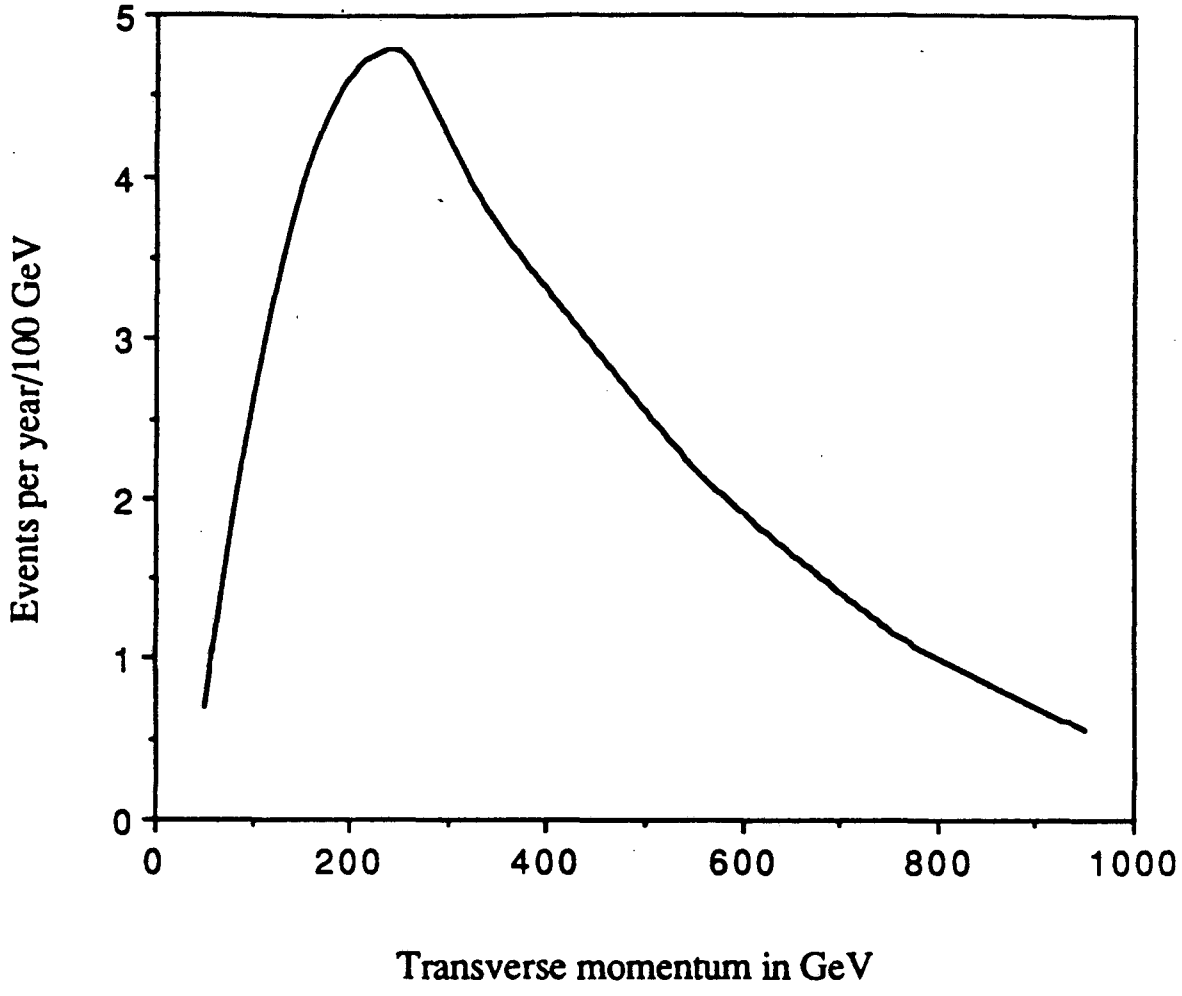


8.8 The $P_T$ distribution of the lepton with the larger $P_T$ from $W^+W^+$ events for $|y_W| < 1.5$ and $m_{WW} > 0.5$ TeV as predicted by the model of Chanowitz and Gaillard (Ref. 4).

There are no other important sources of $W^+W^+$ in the standard model, so that, although the event rates of Fig. 8.8 are small, detection may be possible. Backgrounds in the $W^+W^+$ and $W^-W^-$ channels are likely to be equal whereas the $W^+W^+$ rate from stongly interacting gauge bosons is approximately three times that from $W^-W^-$.[17] Background from events with $W^\pm$ + jet(s) wherein the jets yield an isolated lepton has not been evaluated.

## 9. Conclusions

In this paper we have explored the observability of a heavy Higgs boson at the SSC. We conclude that:

- The heavy Higgs boson may be observed at the SSC up to masses of 600–800 GeV in the mode $H \rightarrow ZZ, Z \rightarrow ee$ or $\mu\mu$. The range results from uncertainties in the $t$ quark mass and our inability to quantify the $ZZ$ continuum background.
- The heavy Higgs boson may be observable for higher masses in the mode $H \rightarrow ZZ, Z \rightarrow ee$ or $\mu\mu$ and $Z \rightarrow \nu\bar{\nu}$ if detectors of sufficient hermeticity can be constructed and operated. A detailed and more realistic study of calorimeter hermeticity and response is required before definite conclusions can be reached.
- The feasibility of detecting the Higgs in the $WW$ mode has not yet been adequately demonstrated here or elsewhere. If the $t$ quark can decay into a real $W$, the $WW$ background will be overwhelming. Studies going beyond partonic level calculations which include fragmentation effects and realistic modeling of calorimeter response are required.
- Detection of $W^{\pm}W^{\pm}$ pairs and $WZ$ events is important and requires more studies at the Monte Carlo level.

The general detector parameters for detection of heavy Higgs decays have been described. Considerable effort will be needed to fine-tune these requirements and to assess the feasibility of construction of actual experiments which meet them.

## References


1. S. Weinberg, Phys. Rev. Lett. 19 (1967) 264; A. Salam, Elementary Particle Physics, ed. N. Svartholm, p. 367.
2. See for example, I. Hinchliffe, Ann. Rev. Nuc. Part. Sci. 36 (1986) 505.
3. S. Weinberg, Phys. Rev. D13 (1976) 974; Phys. Rev D19 (1977) 1277; L. Susskind, Phys. Rev. D20 (1979) 2619.
4. M. Chanowitz and M. Gaillard, Nucl. Phys. B261 (1985) 379.
5. B. Lee, C. Quigg, and H. Thacker, Phys. Rev. D16 (1977) 1519.
6. S. Weinberg, Phys. Rev. Lett. 17 (1966) 616.
7. H. Georgi et al. Phys. Rev. Lett. 40 (1978) 692.
8. R. Cahn and S. Dawson, Phys. Lett. 136B (1984) 196.
9. J.F. Gunion et al., Univ. of California Davis preprint 86-15 (1986).
10. M. Chanowitz and M. Gaillard, Phys. Lett. 142B (1984) 85; S. Dawson, Nucl. Phys. B249 (1985) 42; G. Kane, W. Repko and W. Rolnick, Phys. Lett. 148B (1984) 367.
11. R. Cahn, Nucl. Phys. B255 (1985) 341.

12. J. Gunion and M. Soldate, Phys. Rev. D34 (1986) 826.

13. J. Cornwall, D. Levin and M. Tiktopolous, Phys. Rev. D10 (1974) 1145.

14. M. Bento and C.H. Llewellyn Smith, Nucl. Phys. B289 (1987) 36; G. Altarelli, B.. Mele, and F. Pitolli, Nucl. Phys. B287 (1987) 205; M. Duncan, G. Kane, and W. Repko, Nucl. Phys. B272 (1986) 517.

15. M. Bento and C.H. Llewellyn Smith, *op. cit.*.

16. J. Fleischer and F. Jegerlehner, Phys. Rev. D23 (1981) 2001.

17. M. Chanowitz and M. Golden, in preparation; M. Chanowitz, in the Proceedings of the UCLA Workshop on Observable Standard Model Physics at the SSC: Monte Carlo Simulation and Detector Capabilities, H-U. Bengtsson, C. Buchanan, T. Gottschalk and A. Soni, eds., World Scientific Publishing, Singapore (1986).

18. F. Paige and S. Protopopescu, to appear in in the Proceedings of the UCLA Workshop on Observable Standard Model Physics at the SSC: Monte Carlo Simulation and Detector Capabilities, H-U. Bengtsson, C. Buchanan, T. Gottschalk and A. Soni, eds., World Scientific Publishing, Singapore (1986).

19. H-U. Bengtsson and T. Sjöstrand, in in the Proceedings of the UCLA Workshop on Observable Standard Model Physics at the SSC: Monte Carlo Simulation and Detector Capabilities, H.-U. Bengtsson, C. Buchanan, T. Gottschalk and A. Soni, eds., World Scientific Publishing, Singapore (1986).

20. R.W. Brown and K. Mikaelian, Phys. Rev. D19 (1979) 922.

21. R.W. Brown, D. Sahdev and K. Mikaelian, Phys. Rev. D20 (1979) 1164.

22. D.A. Dicus, C. Kao, and W.W. Repko, Phys. Rev. D36 (1987) 1570.

23. E. Eichten, I. Hinchliffe, K. Lane and C. Quigg, Rev. Mod. Phys. 56 (1984) 579.

24. J. Owens, in the Proceedings of the 1984 Summer Study on the Design and Utilization of the Superconducting Super Collider, Snowmass, Colorado, 1984.

25. W.K. Tung, in the Proceedings of the 1984 Summer Study on the Design and Utilization of the Superconducting Super Collider, Snowmass, Colorado, 1984.

26. J. Collins, in these Proceedings.

27. J. Collins and D. Soper, Ann. Rev. Nucl. Part. Sci., to appear.

28. R. Cahn, S. Ellis, R. Kleiss, and W. Stirling, Phys. Rev. D35 (1987) 1626.

29. D.A. Dicus and R. Vega, Phys. Rev. Lett. 57 (1986) 1110; J.F. Gunion, J. Kalinowski, and A. Tofighi-Niaki, Phys. Rev. Lett. 57 (1987).

30. H-U. Bengtsson, private communication.

31. The branching ratio formulae are conveniently summarized in R. Thun et al., "Searching for the Higgs $\rightarrow Z^0Z^0 \rightarrow \mu^+\mu^-\mu^+\mu^-$ at SSC," in these Proceedings.

32. D. Froidevaux in "Experimental Studies" in the Proceedings of the Workshop on Physics at Future Accelerators, Vol. 1, CERN 87-07.

33. V. Barger, T. Han and R.J.N. Phillips, University of Wisconsin Preprint MAD/PH/368 (revised), September 1987 and references therein.

34. R. Kleiss and W.J. Stirling, CERN-TH-4828-87.

35. A. Savoy-Navarro, contribution to these Proceedings and D. Hedin, private communication.

36. See the reports of the Higgs and $W$ Pair Physics Group in the Proceedings of the Summer Study on the Physics of the Superconducting Super Collider, Snowmass, 1986.

37. F.E. Paige, in the Proceedings of the 1984 Summer Study on the Design and Utilization of the Superconducting Super Collider, Snowmass, Colorado; J.F. Gunion, Z. Kunszt and M. Soldate, Phys. Lett. 163B (1985) 389; Erratum-ibid. 168B (1986) 427; W.J. Stirling, R. Kleiss and S.D. Ellis, Phys. Lett. 163B (1985) 261.

38. J.F. Gunion et al., in the Proceedings of the UCLA Workshop on Observable Standard Model Physics at the SSC: Monte Carlo Simulation and Detector Capabilities.

39. G. Herten, in these Proceedings.

40. F. Paige, "ELMUD: An Electron Muon Detector for Higgs Physics at the SSC," to appear in the Proceedings of the Workshop, from Colliders to Supercolliders, Madison, 1987.

41. M. Chen et al., "High $P_T$ Weak Bosons as Signatures for Higgs-like Heavy Particles," in these Proceedings.

42. Report of the Particle ID Group in the Proceedings of the Workshop on Physics at Future Accelerators, Vol. 1, CERN 87-07.

43. J. Freeman and C. Newman-Holmes, "Detector Dependent Contributions to Jet Resolution," in these Proceedings.

44. R. Cahn and M. Chanowitz, Phys. Rev. Lett. 56 (1986) 1327.

*LAWRENCE BERKELEY LABORATORY*
*TECHNICAL INFORMATION DEPARTMENT*
*UNIVERSITY OF CALIFORNIA*
*BERKELEY, CALIFORNIA 94720*